Entangling Nuclear Spins in Distant Quantum Dots via an Electron Bus

Miguel Bello ⃝,[1,2,*] Mónica Benito,[3] Martin J. A. Schuetz,[4,5,†] Gloria Platero ⃝,[1] and Géza Giedke ⃝[6,7]

[1]*Instituto de Ciencia de Materiales de Madrid (ICMM-CSIC), ES-28049 Madrid, Spain*
[2]*Max Planck Institute of Quantum Optics, DE-85748 Garching, Germany*
[3]*Department of Physics, University of Basel, CH-4056 Basel, Switzerland*
[4]*Amazon Quantum Solutions Lab, Seattle, Washington, DC 98170, USA*
[5]*AWS Center for Quantum Computing, Pasadena, California 91125, USA*
[6]*Donostia International Physics Center (DIPC), ES-20018 Donostia-San Sebastián, Spain*
[7]*IKERBASQUE, Basque Foundation for Science, ES-48013 Bilbao, Spain*

We propose a protocol for the deterministic generation of entanglement between two ensembles of nuclear spins surrounding two distant quantum dots. The protocol relies on the injection of electrons with definite polarization, their sequential interaction with the nuclear ensembles of each quantum dot for a short time, and the coherent transfer of each electron from one quantum dot to the other. Computing the exact dynamics for small systems, and using an effective master equation and approximate nonlinear equations of motion for larger systems, we are able to confirm that our protocol indeed produces entanglement for both homogeneous and inhomogeneous systems. Last, we analyze the feasibility of our protocol in several current experimental platforms.

I. INTRODUCTION

Electron spin coherence in quantum dots is affected by several phenomena, including hyperfine interaction with surrounding nuclei [1–3]. For this reason, scientists have developed various techniques (spin echo, nuclear polarization, or nuclear state narrowing, etc.) to reduce the effects of hyperfine interaction [4,5], or to get rid of the nuclear spins altogether [6]. Going the opposite way, different works have explored the idea of harnessing the long coherence times [recently demonstrated for quantum dots (QDs) experimentally [7, 8]], and slow dynamics of the nuclear spin ensembles [9–18], which make them good candidates for long-time quantum information storage platforms (demonstrated both theoretically [19–22] and experimentally [8,23,24]).

In this work, we follow the latter research line and propose a protocol to produce entanglement between

two distant nuclear ensembles dissipatively and deterministically. This has been pursued in Refs. [25,26] for the two nuclear ensembles surrounding an exchange-coupled double quantum dot. For an analogous operation at longer distances (without direct interaction), as explored in Refs. [27,28] for entanglement generation between distant electrons, one may use a coherent electron bus, such as an array of quantum dots [29–32], a chiral quantum-Hall-effect channel [27], or surface acoustic waves [33–35]. The idea behind most of these proposals is that the moving qubits (a current of electrons) act as a joint bath, whose overall effect is to induce the decay of the system towards a target steady state. By engineering the bath we can modify the properties of this steady state, in particular, we can ensure that the two parties (the two electron spins or two ensembles of nuclear spins) are entangled.

Our work comprises a proposal for entanglement generation between *distant* ensembles of nuclear spins connected via an electron bus. Two different regimes are of potential interest to apply our scheme: on the one hand, the large nuclear ensembles that surround QDs fabricated with GaAs, (In, Ga)As, and ^{29}Si-rich Si, with a number of spins ranging from 100 to 10^6 [36]; on the other, nuclear ensembles with just a few nuclei (< 10) present, for example, in purified Si [24,37]. We also discuss how to detect the entanglement experimentally using different entanglement witnesses suitable for each case.

---

*miguel.bello@mpq.mpg.de
†This work was done prior to joining AWS.

II. DESIGN OF THE PROTOCOL

A. System

Our protocol is designed for a device such as that shown schematically in Fig. 1: two QDs, henceforth labelled as QD1 and QD2, are connected to electron reservoirs so that electrons with definite polarization can be injected into each QD, and they can be released from either QD at will. Furthermore, the two QDs are connected to each other via a coherent electron bus, which can transport electrons from QD1 to QD2.

If QDj is occupied by an electron, the nuclei in a small volume around it will interact with it via the hyperfine interaction [1]. We consider the Fermi contact interaction between an s-type conduction-band electron and the nuclear spins, which is given by the Hamiltonian [1]

$$
\begin{aligned}
H_j &= g_j \mathbf{A}_j \cdot \mathbf{S}_j \\
&= g_j A_j^z S_j^z + \frac{g_j}{2}(A_j^+ S_j^- + A_j^- S_j^+) \\
&\equiv H_j^z + H_j^\perp.
\end{aligned}
\tag{1}
$$

Here, $\mathbf{S}_j$ denotes the electronic spin, while $\mathbf{A}_j = \sum_{i=1}^{N_j} g_{ij} \mathbf{I}_{ij}$ is a collective nuclear spin operator; $\mathbf{I}_{ij}$ is the spin of the ith nucleus in QDj. The ladder operators are defined as usual, $S_j^\pm = S_j^x \pm i S_j^y$ (analogously for $A_j^\pm$). We consider spin-I nuclei, and a total of N_j nuclei in each ensemble. The dimensionless coupling constants g_{ij} may differ depending on the electronic wave function at the positions of the nuclei and the nuclear species. They are normalized such that $\sum_i g_{ij}^2 = 1/(2I)$ [38]. The constants $g_j = A_H / \sum_i g_{ij}$ set the overall strength of the hyperfine interaction in each QD; A_H is a constant that depends
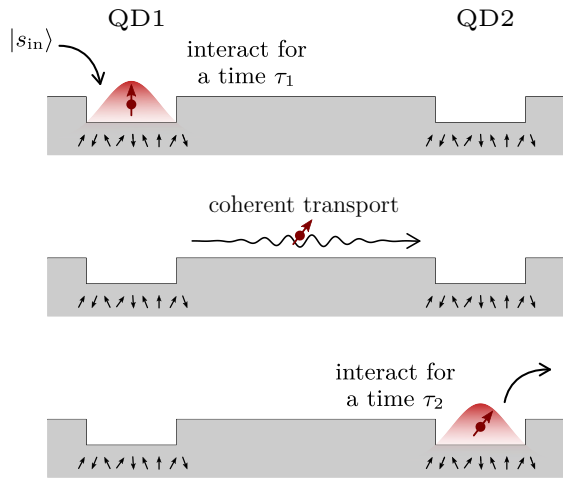

FIG. 1. Schematics of the system under consideration and the manipulations performed in each step of the protocol.

on the material and the density (concentration) of nuclei around the QD [1,39].

Within this model there are several implicit approximations. We assume that the electron injection (retrieval) process is fast on the scale of the hyperfine interaction, so that H_j is switched on (off) abruptly whenever an electron is added to (removed from) QDj, and that it is spin independent [34]. We also neglect other effects, such as noncontact terms of the hyperfine interaction and nuclear dipole-dipole interactions, which are usually much weaker compared with the contact interaction [40,41]. To gain analytical insight into the performance of the protocol, we neglect spin-orbit coupling, which is weak in GaAs, and all electron spin decoherence processes, which are, nonetheless, considered in some of the numerical calculations. These simplifications and the consequences of relaxing some of them are discussed and justified in Sec. V.

B. Protocol

The protocol consists of a sequence of fast interactions with a sequence of independent, individually injected, polarized electrons that generate a dissipative dynamics whose principal (Lindbladian) terms stabilize a spin-squeezed state of the two ensembles, similar to analogous protocols realized in quantum optics [42,43]. Specifically, the protocol consists in the repetition of a cycle comprised of $2 + 2k$ steps ($k \geq 1$), summarized in Table I. At the beginning of the nth step, a new electron with definite polarization is injected into QD1 in state $|s_{\text{in}}^{(n)}\rangle$. This electron interacts with the nuclei in QD1 for a certain period of time τ_1 and then it is transported to QD2, where it interacts with the nuclei there for a period τ_2; see Fig. 1. At the end of each step the electron in QD2 is released from the device, leaving the two QDs ready to start a new step. Ideally, the dwell times τ_1 and τ_2, and the polarization of the injected electrons at each step are required to fulfill a specific pattern: in the first step (injected spin "up") $g_1 \tau_1 = \mu$ and $g_2 \tau_2 = \nu$, with $\tau_1 > \tau_2$ ($|\mu| > |\nu|$), while in the second step (injected spin "down") $g_1 \tau_1 = \nu$ and $g_2 \tau_2 = \mu$. The difference between μ and ν induces a term of strong dephasing that will be canceled by the remaining $2k$ steps, where each nuclear ensemble evolves independently under the influence of k consecutive electrons, all with the same polarization ("down" for QD1 and "up" for QD2), that each spend a short time $\tau_j \propto k^{-1}$ trapped in QDj.

The rationale behind this particular choice of the dwell times and injected electron states is the following. For short dwell times, we can neglect higher-order terms in the hyperfine interaction and each electron flips at most once when interacting with the nuclear ensembles. In the first two steps of the protocol, each electron is transported coherently between QD1 and QD2, such that interference between the "flipped in QD1" and "flipped in QD2" paths

TABLE I. Single cycle of the protocol, comprising $2k + 2$ steps, where the nth step begins with the injection of an electron in state $|s_{\text{in}}^{(n)}\rangle$ into QD1, where it remains for time $\tau_1^{(n)}$ to accumulate an effective interaction $g_1 \tau_1^{(n)}$, and is then transported to QD2 via the quantum channel $\mathcal{E}$ and interacts with its nuclear ensemble for a time $\tau_2^{(n)}$. The third and fourth rows are steps repeated a total of k times each. In the ideal case, the electron would be transported coherently without dissipation ($\mathcal{E}[\rho_{\text{el}}] = \rho_{\text{el}}$) and the dwell times would be such that $\mu_1 = \mu_2 \equiv \mu$ and $\nu_1 = \nu_2 \equiv \nu$.

Step	Injected state $|s_{\text{in}}^{(n)}\rangle$	Interaction QD1 $g_1 \tau_1^{(n)}$	Quantum channel	Interaction QD2 $g_2 \tau_2^{(n)}$
1	$|\uparrow\rangle$	μ_1	$\mathcal{E}$	ν_2
2	$|\downarrow\rangle$	ν_1	$\mathcal{E}$	μ_2
$3, \ldots, 2+k$	$|\downarrow\rangle$	$(\mu_1 - \nu_1)/k$	$\ldots$	0
$3+k, \ldots, 2+2k$	$|\uparrow\rangle$	0	$\ldots$	$(\mu_2 - \nu_2)/k$

occurs. This uncertainty regarding where the electrons have flipped will be mapped onto an entangled nuclear state after tracing out (discarding) the electrons. Simultaneously, these two steps produce unwanted dynamics due to the zz-hyperfine terms. On the nuclei, these latter terms act like an (in general inhomogeneous) effective magnetic field (the Knight field) that can be canceled with additional local terms, which are produced in the remaining steps of each cycle.

To keep our equations general (e.g., to cover cases where g_j is not exactly known or the effective g_j depends on the nuclear state), we consider in the following the possibility of having different constants $\{\mu_j, \nu_j\}$ for each QD ($j = 1, 2$); see Table I. Also, in an actual experiment, the electron transport from QD1 to QD2 in the first two steps of each cycle may suffer mostly from decoherence (due to hyperfine interaction with intervening nuclear spins between the two QDs). To model these imperfections, one can use a quantum channel $\mathcal{E}$ acting on the electronic degrees of freedom. Further details are given in Sec. V.

Let us derive the most general evolution after a single step of our protocol. The induced nuclear dynamics is stroboscopic, in the sense that the nuclei only evolve whenever they interact with an electronic spin. After the $(n-1)$th step the electron is discarded and the nuclei remain in the (generally mixed) state ρ_{n-1}. The injection of a new electron, with state $|s_{\text{in}}^{(n)}\rangle$, at the beginning of the nth step transforms the density matrix of the system as $\rho_{n-1} \to \chi_{n-1} = \rho_{n-1} \otimes |s_{\text{in}}^{(n)}\rangle \langle s_{\text{in}}^{(n)}|$. Then, interaction between the electron spin and the first nuclear ensemble produces $\chi_{n-1} \to e^{-i\tau_1^{(n)} H_1} \chi_{n-1} e^{i\tau_1^{(n)} H_1} = e^{\tau_1^{(n)} \mathcal{L}_1}[\chi_{n-1}]$, where $\mathcal{L}_j[\chi] = -i[H_j, \chi]$ is the Liouvillian corresponding to the coherent evolution given by the hyperfine interaction in the jth QD. Transport of the electron between QD1 and QD2 results in $e^{\tau_1^{(n)} \mathcal{L}_1}[\chi_{n-1}] \to \mathcal{E}[e^{\tau_1^{(n)} \mathcal{L}_1}[\chi_{n-1}]]$, and interaction between the electron and the nuclei in QD2 is given by the same transformation as the interaction in QD1, simply replacing $\tau_1^{(n)}$ and H_1 by $\tau_2^{(n)}$ and H_2. Finally, the nuclei's reduced density matrix after discarding the electron state is

given by

$$\rho_n = \text{tr}_{\text{el}}(e^{\tau_2^{(n)} \mathcal{L}_2}[\mathcal{E}[e^{\tau_1^{(n)} \mathcal{L}_1}[\chi_{n-1}]]]). \quad (2)$$

As can be seen, this stroboscopic evolution is Markovian by construction, since the future state of the nuclei, ρ_n, depends only on the current state ρ_{n-1}. This is due to the fact that the electrons are discarded at the end of each step, and new electrons, which have not interacted previously with the nuclei, are injected at the beginning of each step. So they can be regarded as a "memoryless" environment for the nuclei.

Additionally, we require the interaction times to be short in comparison with the typical hyperfine-interaction timescales. More specifically, $\tau_j^{(n)} < \|H_j\|^{-1}$, where $\|\cdot\|$ denotes the operator norm (i.e., $\tau_j^{(n)} < 2I^{-1} A_H^{-1}$). If that is the case, we can approximate the dynamics by truncating the Taylor expansion of the exponentials up to second order. Then, the change in the density matrix after a single cycle is given by (see Appendix A)

$$\Delta\rho \simeq \frac{(\mu - \nu)^2}{4k} \{\mathcal{D}(A_1^-) + \mathcal{D}(A_2^+)\}[\rho]$$

$$+ \frac{1}{4} \{\mathcal{D}(\mu A_1^+ + \nu A_2^+) + \mathcal{D}(\nu A_1^- + \mu A_2^-)\}[\rho], \quad (3)$$

where $\mathcal{D}(X)[\rho] \equiv X\rho X^\dagger - \{X^\dagger X, \rho\}/2$, and we have assumed perfect control of the dwell times ($\mu_1 = \mu_2 = \mu$, $\nu_1 = \nu_2 = \nu$) and perfect electron transfer ($\mathcal{E}[\chi] = \chi$ for all χ). In the remainder, we focus on the ideal case given in Eq. (3), while the effect of small deviations from this case is considered in Sec. V.

III. ENTANGLEMENT CRITERIA

To detect entanglement between the two nuclear ensembles in an experiment one can employ a spin-squeezing criterion [25,42] based on the following principle [44]. Given two observables X_j and Y_j of each ensemble $j = 1, 2$ satisfying the commutation relation $[X_i, Y_j] = \delta_{ij} Z_j$, and linear

combinations $u = \alpha X_1 + \beta X_2$ and $v = \alpha Y_1 - \beta Y_2$, then, for any separable state, the inequality

$$\text{var}(u) + \text{var}(v) \geq \alpha^2 |\langle Z_1 \rangle| + \beta^2 |\langle Z_2 \rangle| \qquad (4)$$

holds. Choosing $\alpha = \beta = 1$, $X_j = J_j^x$, and $Y_j = (-1)^{j+1} J_j^y$, where J_j^ν is the ν component ($\nu = x, y, z$) of the total nuclear angular momentum $\mathbf{J}_j \equiv \sum_i \mathbf{I}_{ij}$, we conclude that if $\Delta_{\text{EPR}} < 1$, where

$$\Delta_{\text{EPR}} \equiv \frac{\text{var}(J_1^x + J_2^x) + \text{var}(J_1^y + J_2^y)}{|\langle J_1^z \rangle| + |\langle J_2^z \rangle|} \qquad (5)$$

is the so-called EPR uncertainty, then there is entanglement between the two nuclear ensembles. Note that this is a sufficient condition for the state to be entangled, but it is not necessary, i.e., there are entangled states that cannot be detected by this criterion. Experimentally, this criterion requires the measurement of the nuclear polarizations of each ensemble. The small size of the nuclear ensemble makes this quite challenging with NMR techniques [45].

Instead, the most natural way to measure observables of the nuclear spin ensemble in a QD is via the interaction with the electron spin, i.e., by measuring the Overhauser field [3]. This allows us to magnify the small nuclear signal and ensures that only spins actually coupled to the electron contribute. This technique, however, does not give access to the total nuclear spin operators if the couplings are inhomogeneous. But the principle described in Eq. (4) also applies to the collective operators $\mathbf{A}_j$; the variances of nonlocal operators involving $A_j^{x,y}$ then have to be compared to expectation values of $[A_j^x, A_j^y] = iA_j^{(z,2)}$, where we set $A_j^{(z,2)} \equiv \sum_i g_{ij}^2 I_{ij}^z$. Thus, we define a new quantity

$$\Delta \equiv \frac{\text{var}(A_1^x + A_2^x) + \text{var}(A_1^y + A_2^y)}{|\langle A_1^{(z,2)} \rangle| + |\langle A_2^{(z,2)} \rangle|}, \qquad (6)$$

for which it still holds that $\Delta < 1$ implies that the two ensembles are entangled. To avoid confusion, we refer to the expectation value $\langle J_j^z \rangle / (N_j I)$ simply as the polarization of the jth ensemble, while we refer to $2\langle A_j^{(z,2)} \rangle$ as the generalized polarization. Because of our choice of normalization for the g_{ij}, the range of this quantity will be $[-2I, 2I]$ for spin-I nuclei for both $j = 1, 2$. Also, note that, for an homogeneous system with identical ensembles ($N_1 = N_2$), both Δ_{EPR} and Δ are equal.

Besides the criteria discussed here, there are many other ones one could employ to detect bipartite entanglement experimentally, for example criteria based on the covariance matrix [46,47]. For small nuclear spin ensembles, and if the full nuclear density matrix can be determined, one could employ criteria based on the negativity, or other entanglement witnesses. For example, for two single-spin-1/2 ensembles one could detect entanglement measuring the singlet occupation [48] (see Appendix B).

IV. DYNAMICS

A. Homogeneous case

First, note that in the homogeneous case, i.e., when all nuclear spins belonging to the same ensemble couple with the same strength to the electronic spin ($g_{ij} = 1/\sqrt{2IN_j}$ for all $i = 1, \ldots, N_j$), the collective nuclear spin operators form a spin algebra $\mathbf{A}_j \propto \mathbf{J}_j$, and the total angular momentum of each ensemble $J_j \in \{N_j/2, N_j/2 - 1, \ldots, (N_j \mod 2)/2\}$ is conserved throughout evolution. Thus, the density matrix can be split into blocks corresponding to different sectors (subspaces) with different values of (J_1, J_2) that evolve independently, and the steady state has no correlations between these blocks.

Let us start by analyzing the dynamics in a simple limiting case. The last two dissipators of Eq. (3) drive the spin ensembles towards an entangled steady state, while the first two dissipators locally depolarize the nuclear spin ensembles and are detrimental for entanglement generation. If evolution were dictated by just the second line of Eq. (3) (as it is in the limit $k \to \infty$) then the steady state in the subspaces with equal total angular momenta $J_1 = J_2 = J$ would be a two-mode spin squeezed state [49], given by the pure (unnormalized) state

$$|\Psi_{\text{TMS}}\rangle = \sum_{n=0}^{2J} \left(-\frac{\nu}{\mu} \right)^n |J, J-n\rangle_1 |J, n-J\rangle_2, \qquad (7)$$

written here in terms of Dicke states $|J, M\rangle_j$ [50], which are eigenstates of $\mathbf{J}_j^2$ and J_j^z with eigenvalues $J(J+1)$ and M, respectively. In this state, for sufficiently different μ and ν, the two nuclear ensembles are highly polarized in opposite directions, and the EPR uncertainty turns out to be independent of J, $\Delta_{\text{EPR}} = (\mu - \nu)^2 / |\mu^2 - \nu^2|$; hence, $\Delta_{\text{EPR}} < 1$ for $\mu\nu > 0$, so the steady state is entangled. For unequal total angular momenta $J_1 \neq J_2$, the steady state corresponding to the dissipators in the second line of Eq. (3) is not pure, although still entangled [26]. For nonmaximal J_1, J_2, the steady state is not unique, but the (spin permutation) quantum numbers associated with this nonuniqueness [50] are conserved by the homogeneous dynamics and do not affect the EPR uncertainty, so they can be ignored.

By increasing the number of steps per cycle (making k larger), we are able to bring the actual steady state of Eq. (3) closer to $|\Psi_{\text{TMS}}\rangle$ (see Appendix B). There is, however, a physical limitation on how small the dwell times can be made while still retaining control of the process. For example, in Ref. [34], the injection and ejection pulses take about 90 ps, and the time jitter is quoted as 6.6 ps. Nonetheless, as we show in the following, the protocol also works for small values of k (even for $k = 1$).

For the more general case, considering a finite value of k, and arbitrary, large initial total angular momenta J_j, we

can obtain an analytical estimate of Δ_{EPR} by bosonizing the excitations of each ensemble over the fully polarized states $|J_1, J_1\rangle_1$ and $|J_2, -J_2\rangle_2$ via the Holstein-Primakoff (HP) transformation [51], which maps spin operators $\mathbf{J}_j$ to bosonic operators a_j, $a_j^\dagger$ as

$$J_1^z = J_1 - a_1^\dagger a_1, \quad J_1^+ = \sqrt{2J_1 - a_1^\dagger a_1}\, a_1, \qquad (8)$$

$$J_2^z = a_2^\dagger a_2 - J_2, \quad J_2^- = \sqrt{2J_2 - a_2^\dagger a_2}\, a_2. \qquad (9)$$

Note that the role of the ladder operators is reversed in QD2. If $\langle a_j^\dagger a_j \rangle \ll J_j$, we can approximate

$$A_1^+ = \frac{J_1^+}{\sqrt{2N_1 I}} \approx \sqrt{r_1}\, a_1, \quad A_2^- = \frac{J_2^-}{\sqrt{2N_2 I}} \approx \sqrt{r_2}\, a_2, \quad (10)$$

and similarly $A_1^- \approx \sqrt{r_1}\, a_1^\dagger$ and $A_2^+ \approx \sqrt{r_2}\, a_2^\dagger$, where $r_j = J_j/(N_j I)$ is the ratio between the total spin and the maximum possible total spin for the jth ensemble. Rewriting Eq. (3) using this transformation we obtain a new master equation whose steady state can be found analytically (see Appendix C).

For $k = 1$, the EPR uncertainty in the steady state reads

$$\Delta_{\text{EPR}}^{\text{HP}} = \frac{\mu^2}{4\kappa} - 1 - \frac{\sqrt{J_1 J_2}}{(J_1 + J_2)} \frac{\sqrt{r_1 r_2}}{(r_1 + r_2)} \frac{\mu\nu}{\kappa}, \qquad (11)$$

where $\kappa \equiv (\mu\nu - \nu^2)/4 > 0$. Considering the relation between the arithmetic and geometric means, we can readily see that $\Delta_{\text{EPR}}^{\text{HP}}$ is smaller the more similar the total spins J_1 and J_2 are, and also the more similar the ratios r_1 and r_2 are. In Fig. 2(a) we plot this quantity for the subspace with maximal total angular momenta ($J_j = N_j I$), showing the values of N_1/N_2 and ν/μ for which we expect to detect entanglement in the steady state.

In addition, this bosonization approach allows us to compute the dynamics, provided the conditions $\langle a_j^\dagger a_j \rangle \ll J_j$ are satisfied at all times. This is indeed the case for sufficiently small ν/μ and for the fully polarized initial state $|\Psi_{\text{FP}}\rangle = |\Uparrow\rangle_1 |\Downarrow\rangle_2$, $\rho_0 = |\Psi_{\text{FP}}\rangle \langle \Psi_{\text{FP}}|$ (where $|\Uparrow\rangle_j$, $|\Downarrow\rangle_j$ denote the states in which all nuclei in QDj are polarized "up" or "down," respectively). The resulting dynamics approaches the steady-state polarization exponentially with rate κr_j in each QD (see Appendix C). Our simulations indicate that the timescale on which the steady state is reached is close to the polarization timescale of the individual ensembles. In the case where both ensembles are initially highly polarized ($r_1, r_2 \simeq 1$), this timescale is approximately given by $T_{\text{stab}}^{\text{hom}} \simeq 1/(2\kappa)$.

In Fig. 2(b) we compare the steady-state polarizations and Δ_{EPR} obtained by means of the exact dynamics, Eq. (2), with those obtained using the second-order master equation, Eq. (3), for a system consisting of two identical, homogeneous ensembles (initially fully polarized). While the polarizations do not present visible differences, there is some discrepancy between both in terms of
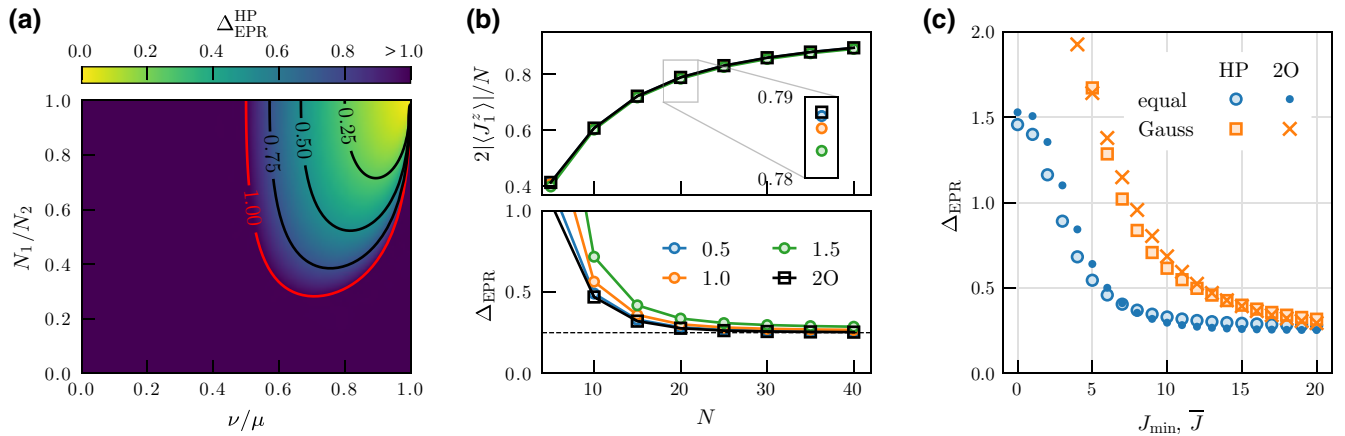

FIG. 2. (a) Contour plot of $\Delta_{\text{EPR}}^{\text{HP}}$, Eq. (11), for the subspace with maximal total angular momenta $J_j = N_j I$ ($r_j = 1$). (b) Characterization of the steady state in the subspace with maximum total angular momenta as a function of the number of nuclei for two identical ($N_1 = N_2 \equiv N$), homogeneous ensembles of spin-1/2 nuclei. We compare the exact dynamics (circles) with the result given by the second-order (2O) master equation (squares) for several different values of $\mu\sqrt{N}$, as indicated in the legend. The result given by the master equation does not depend on the individual values of μ and ν but only on their ratio. For all the curves plotted, this ratio is the same, $\nu/\mu = 0.8$. The dashed horizontal line marks the value obtained by the Holstein-Primakoff approximation in the limit $J_j \to \infty$, $\Delta_{\text{EPR}}^{\text{HP}}$. (c) Steady-state Δ_{EPR} for an initial mixed state: blue circles and dots correspond to an initial equal-weight mixture of all states with $J_1, J_2 \geq J_{\text{min}}$, while orange squares and crosses correspond to an initial state with a Gaussian probability distribution, $p_j(J) \propto \exp[-(J - \bar{J})^2/(2w^2)]$, of the total angular momenta with mean $\bar{J}$ and variance $w^2 = 3$. The system is the same as in panel (b), with $N = 40$ spins. The ratio $\nu/\mu = 0.8$ is the same for all the points. The results have been obtained using the Holstein-Primakoff approximation and the second-order master equation.

entanglement, which is reduced by making the interaction times smaller. As we can see, Δ_{EPR} decreases monotonically as we increase N (J_j), and the approximation $\Delta_{\text{EPR}}^{\text{HP}}$ already agrees well with the result of the master equation for $N \gtrsim 25$. Thus, in order to obtain the maximum amount of entanglement, it is preferable that initially the subspace with largest occupation be the one with maximum total angular momenta $(J_1, J_2) = (N_1 I, N_2 I)$. This requirement on the initial state could be enforced by fully polarizing the two nuclear ensembles, a task for which many protocols have been devised (e.g., Refs. [16,52–55]) and towards which significant experimental progress has been reported [5,56–58]. Some limitations to dynamical nuclear polarization have also been predicted [59].

We can easily extend these results to nonmaximal J_j and even to mixed initial states. For example, we may consider an initial state of the form $\rho_0 = \rho_{\text{QD1}} \otimes \rho_{\text{QD2}}$, with $\rho_{\text{QD}j} = \sum_J p_j(J) \rho_j(J)$. Here, $\rho_j(J)$ is some normalized density matrix that belongs to the subspace of states of the jth nuclear ensemble with total angular momentum J, and $p_j(J)$ is some discrete probability distribution. Since the steady state within each fixed angular momenta subspace is unique (up to variations of the permutation quantum numbers), the steady-state value of Δ_{EPR} depends only on the initial distributions $p_j(J)$. In Fig. 2(c) we show the resulting steady-state Δ_{EPR} for an initial Gaussian distribution and also for an equal-weight mixture of all states with $J_1, J_2 \geq J_{\min}$, demonstrating that maximal polarization of the nuclear ensembles is not strictly required for the protocol to work (see Appendix C).

B. Inhomogeneous case

As explained in the beginning of Sec. IV A, the homogeneous case is numerically simpler because of the conservation of total angular momentum. In the inhomogeneous case, the total angular momentum of each nuclear ensemble is not conserved and we have to consider the full Hilbert space of the two nuclear ensembles in order to compute the dynamics exactly. This limits the direct application of Eq. (2) or (3) to very small systems (which may, however, still be relevant for experiments). Henceforth, we consider spin-1/2 nuclei, $I_{ij}^\alpha = \sigma_{ij}^\alpha/2$ ($\alpha = x, y, z$). In Fig. 3 we show the expected dynamics for a system with only two spins in each QD, considering both homogeneous and inhomogeneous couplings. For inhomogeneous couplings, the criterion based on Δ fails to detect entanglement, yet the steady state is entangled, as can be demonstrated by the positive partial transpose (PPT) criterion [60–62].

For larger ensembles, we concentrate instead on the quantities required to compute Δ, i.e., $\langle A_{1,2}^{(z,2)} \rangle$ and $\text{var}(A_1^{x,y} + A_2^{x,y})$. They depend on the elements of the covariance matrix $\gamma_{ii'}^{jj'} \equiv \langle \sigma_{ij}^+ \sigma_{i'j'}^- \rangle$ and lower-order terms like $\langle \sigma_{ij}^x \rangle$, whose equations of motion can be derived from
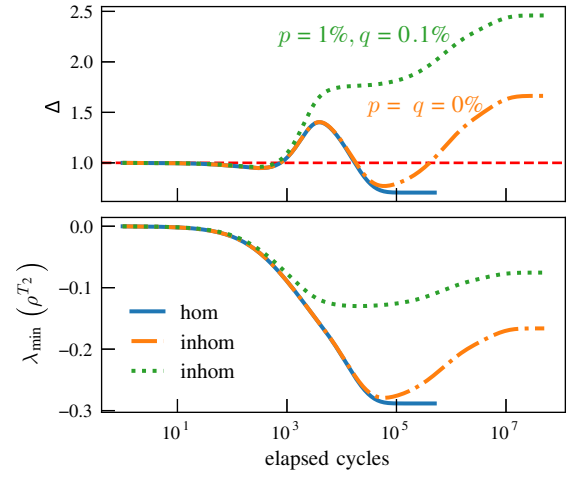

FIG. 3. Simulation of a small system with $N_1 = N_2 = 2$ nuclei in each ensemble computed using the exact dynamics, Eq. (2). The initial state is $|\Psi_{\text{FP}}\rangle$. The rest of the parameters are $\mu = 0.1/\sqrt{N_1}$, $\nu = 0.8\mu$, $k = 5$. Comparison between the homogeneous case, $g_{i1} = g_{j2} = 1/\sqrt{2}$ (blue continuous line), and two cases with a small inhomogeneity, $g_{11} \simeq 0.714$, $g_{21} \simeq 0.7$, $g_{12} \simeq 0.725$, $g_{22} \simeq 0.689$ (green dotted and orange dash-dot lines). In one of the cases shown we also consider imperfect electron spin injection and dephasing during electron transport (green dotted line), with finite p and q; see Sec. V. Even though $\Delta > 1$ for the inhomogeneous cases, the steady state is entangled, as shown in the bottom panel, where we plot the lowest eigenvalue of the partially transposed nuclear density matrix ρ^{T_2}. Note how the small difference between the couplings in the two cases considered only affects the dynamics after many cycles (at long times).

Eq. (3) as (see Appendix D)

$$
\Delta \gamma_{ii'}^{jj'} = \left(\kappa - \frac{\mu^2}{4} \right)(g_{ij}^2 + g_{i'j'}^2)\gamma_{ii'}^{jj'}
$$
$$
+ [\mu^2 \delta_{jj'} + \mu\nu(1 - \delta_{jj'}) - 8\kappa \delta_{j2}\delta_{j'2}]
$$
$$
\times \frac{g_{ij} g_{i'j'}}{4} \langle \sigma_{ij}^z \sigma_{i'j'}^z \rangle + \kappa(-1)^j g_{ij} \sum_{k \neq i} g_{kj} \langle \sigma_{kj}^+ \sigma_{ij}^z \sigma_{i'j'}^- \rangle
$$
$$
+ \kappa(-1)^{j'} g_{i'j'} \sum_{k \neq i'} g_{kj'} \langle \sigma_{ij}^+ \sigma_{i'j'}^z \sigma_{kj'}^- \rangle, \tag{12}
$$

$$
\Delta \lambda_{ii'}^{jj'} = \left[4\kappa(\delta_{j2} g_{ij}^2 + \delta_{j'2} g_{i'j'}^2) - \frac{\mu^2}{2}(g_{ij}^2 + g_{i'j'}^2) \right]\lambda_{ii'}^{jj'}
$$
$$
+ [\mu^2 \delta_{jj'} + \mu\nu(1 - \delta_{jj'}) - 8\kappa \delta_{j2}\delta_{j'2}]g_{ij} g_{i'j'} 2\gamma_{ii'}^{jj'}
$$
$$
- 2\kappa(-1)^j \sum_k g_{kj} g_{ij} (\langle \sigma_{ij}^+ \sigma_{i'j'}^z \sigma_{kj}^- \rangle + \langle \sigma_{kj}^+ \sigma_{i'j'}^z \sigma_{ij}^- \rangle)
$$
$$
- 2\kappa(-1)^{j'} \sum_k g_{kj'} g_{i'j'} (\langle \sigma_{i'j'}^+ \sigma_{ij}^z \sigma_{kj'}^- \rangle
$$
$$
+ \langle \sigma_{kj'}^+ \sigma_{ij}^z \sigma_{i'j'}^- \rangle), \tag{13}
$$

As can be seen in these equations, the elements of the covariance matrix depend on zz correlations, $\lambda_{ii'}^{jj'} \equiv \langle \sigma_{ij}^z \sigma_{i'j'}^z \rangle$ for $(i,j) \neq (i',j')$, and higher-order correlations. Because of the spin-operator commutation relations, and since the Lindblad operators depend on linear combinations of $\sigma_{ij}^\pm$ only, the only higher-order terms occurring in the equations of motion for $\gamma_{jj'}^{ii'}$ and $\lambda_{jj'}^{ii'}$ are of the form $\langle \sigma_i^+ \sigma_j^z \sigma_k^- \rangle$. In order to obtain a tractable system of equations, we make some factorization assumptions that effectively approximate these higher-order correlations in terms of lower-order ones. There are several approximation schemes one can use for this purpose [52]. Among all the approximations we have investigated (see Appendix D), the one that best approximates the dynamics is

$$\langle \sigma_{ij}^+ \sigma_{kl}^z \sigma_{mn}^- \rangle \approx (2\gamma_{kk}^{ll} - 1)\gamma_{im}^{jn} + 2(-1)^l \gamma_{ik}^{jl} \gamma_{km}^{ln} \quad (14)$$

for $(i,j) \neq (k,l) \neq (m,n)$ and $(m,n) \neq (i,j)$.

In Fig. 4(a) we employ these equations of motion to compute the dynamics of a large inhomogeneous system (larger than that shown in Fig. 3, but still much smaller than realized in experiments with typical GaAs or Si QDs). The results show that, for not too inhomogeneous couplings (taken from a Gaussian distribution with large width c; cf. the caption of Fig. 4), the steady state is entangled and that this entanglement can be detected experimentally via Δ. Furthermore, for all cases considered, we find $\Delta < 1$ after some initial cycles, albeit at later times Δ takes on larger values and deviates away from this minimum, reaching $\Delta > 1$ for the more inhomogeneous cases. For moderately inhomogeneous systems, there is a clear distinction between two timescales. On the one hand, there is the timescale in which the system reaches the minimum Δ, which roughly corresponds to the stabilization time of the equivalent homogeneous system, $T_{\text{ent}} \sim (2\kappa)^{-1}$. On the other hand, there is the timescale in which the system reaches the steady state, T_{stab}, which is now much longer than in the homogeneous case. Also, estimating this timescale is harder in the inhomogeneous case, as the dynamics do not follow a simple exponential decay. The dynamics of the generalized polarization of each ensemble, $\langle A_j^{(z,2)} \rangle$, is perhaps the simplest to analyze, as it just depends on the coupling constants within the given ensemble. Numerically, we can show that the stabilization time scales with the smallest difference of the coupling constants of the corresponding ensemble as $T_{\text{stab}} \sim [\mu \min(|g_{ij} - g_{i'j}|)]^{-2}$, see Fig. 4(b), where T_{stab} has been computed as the time in which $\langle A_j^{(z,2)} \rangle_{T_{\text{stab}}} - \langle A_j^{(z,2)} \rangle_\infty = 10^{-3} \langle A_j^{(z,2)} \rangle_\infty$.

Although the use of approximate equations of motion reduces considerably the cost of computing the dynamics, it is possible to reduce it even further considering a "shell model." Formally, a shell model is obtained by discretizing the range of possible values of the coupling constants. We
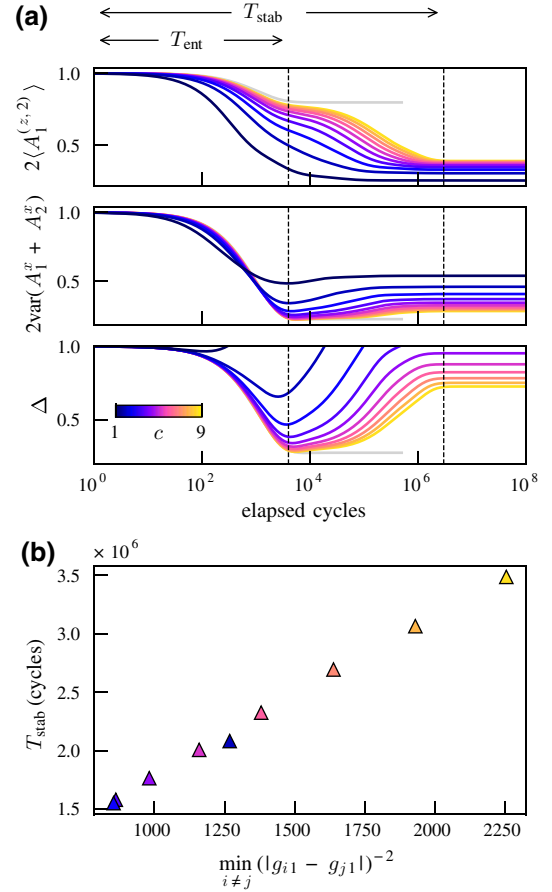

FIG. 4. (a) Dynamics of a shell model with different inhomogeneity degrees (color coded). The couplings follow a Gaussian function $g_{ij} \propto \exp(-\|\mathbf{r}_{ij}\|^2/c)$, where $\{\mathbf{r}_{ij}\}$ denote the positions of the nuclei, which are assumed to form a two-dimensional square lattice, $\mathbf{r}_{ij} \in \mathbb{Z}^2$. We only consider the nuclei within a given distance from the origin $\|\mathbf{r}_{ij}\| < r_j^{\max}$, $r_1^{\max} = 2.5$ and $r_2^{\max} = 3$, resulting in a total of $N_1 = 21$ and $N_2 = 25$ nuclei in each ensemble. The inhomogeneity in each QD is determined by the ratio $c/r_j^{\max}$, such that larger ratios correspond to more homogeneous systems. Parameters are $\mu = 0.5/\sqrt{N_1}$, $\nu = 0.8\mu$, $k = 1$. The initial state is $|\Psi_{\text{FP}}\rangle$. Dashed vertical lines roughly indicate the two different timescales present in the dynamics. Gray curves show the dynamics for an equivalent homogeneous system. (b) Stabilization times for the generalized polarization in QD1 versus the inverse squared smallest nonzero difference between the couplings in QD1. For very inhomogeneous systems, the points obtained (not shown) do not follow this linear dependence. The color code used to denote different inhomogeneity degrees is the same in both panels.

define the shell $\mathcal{S}_{\alpha j}$ as the set

$$\mathcal{S}_{\alpha j} = \{i \in \text{QD}j : g_{ij} \in [g_\alpha, g_{\alpha+1}]\}, \quad (15)$$

where the endpoints of the intervals $\{g_\alpha\}_{\alpha=1,2,...}$ are fixed *a priori*. Then, we approximate the coupling constants of all nuclei within each shell by the average coupling strength

in that shell, $g_{ij} \simeq g_{\alpha j} \equiv |\mathcal{S}_{\alpha j}|^{-1} \sum_{n \in \mathcal{S}_{\alpha j}} g_{nj}$ for all $i \in \mathcal{S}_{\alpha j}$ ($|\mathcal{S}_{\alpha j}|$ denotes the number of elements in the set $\mathcal{S}_{\alpha j}$). In general, a finer discretization would yield more accurate results, valid for a longer time period. More specifically, we expect the dynamics of a shell model to be a good approximation to the actual dynamics of an inhomogeneous system up to an approximate time of $1/\delta g$, where $\delta g = \max_{\alpha, j}(\max_{i \in \mathcal{S}_{\alpha j}} |g_{ij} - g_{\alpha j}|)$.

If initially the covariance matrix elements and *zz* correlations of spins that belong to the same shell are the same, as happens in a fully polarized initial state $\rho_0 = |\Psi_{\text{FP}}\rangle\langle\Psi_{\text{FP}}|$, then they will remain the same throughout the entire time evolution. Therefore, by using a shell model, we can reduce the number of variables, since we only have to consider one representative for each shell.

Besides computing the dynamics, we can directly solve for the steady state, that is, solve the system of equations $\Delta\gamma_{ii'}^{jj'} = 0$ and $\Delta\lambda_{ii'}^{jj'} = 0$. Numerically, we find for a fully polarized ρ_0 that correlations between nuclear spins in different shells of the same QD vanish in the steady state. As a consequence, the steady-state polarization of each shell is independent of the others, and can be found analytically by solving a simple quadratic equation (see Appendix E). Furthermore, the steady-state polarization of each shell depends only on the values of μ, ν, and the number of nuclei in the shell, but not on the specific value of the coupling constants $g_{\alpha j}$. On the other hand, the steady-state value of the transverse spin variance depends continuously on the specific values of the coupling constants.

Although the steady state computed this way will only be exact if the coupling constants of spins within the same shell are actually the same, $\delta g = 0$, the use of a shell model can help us simulate the transient dynamics of very large ensembles. As Figs. 3 and 4 suggest, small variations in the couplings only affect the long-term dynamics, making it possible to have an entangled state at intermediate times for almost any system with sufficiently homogeneous couplings (see Appendix E for further calculations supporting this conclusion).

V. EXPERIMENTAL REALIZATIONS

In this section we discuss the feasibility of our proposal. We review the elements required to build the setup, the most relevant imperfections that may arise in experiment, and the different techniques one can employ to detect the entanglement produced.

A. Necessary ingredients

(1) *Injection of electron spins with definite polarization.* Ferromagnetic leads or spin filters [63–65] can be used for spin-polarized electron injection.

(2) *Coherent transport of electrons.* Great progress has been achieved towards this goal using surface acoustic

TABLE II. Typical time and energy scales for different possible experimental setups. We consider the cases of GaAs QDs, and Si QDs with different concentrations of ^{29}Si. In all the cases shown the parameters of the protocol are the same: $N_1 \simeq N_2 \simeq N$, $\mu = 1.5/\sqrt{2IN}$, $\nu = 0.8\mu$, and $k = 1$. Furthermore, we assume approximately homogeneous couplings $g_{ij} \simeq 1/\sqrt{2IN}$, $g_j \simeq A_H\sqrt{2I/N}$. The time per cycle (taking into account only the dwell times) is given by $\Delta t = 2\mu(g_1^{-1} + g_2^{-1})$, whereas the time in which we expect to produce entanglement is $T_{\text{ent}} \sim (2\kappa)^{-1}$ cycles, which is of the order of about $11IN$ cycles. In the last column we show the nuclear dephasing time due to nuclear dipole-dipole interactions.

Material	N	A_H (μeV)	Δt (ns)	T_{ent} (ms)	T_{dd} (ms)
GaAs	10^5	91.2	0.014	0.024	0.1
20% Si	2×10^4	0.86	5	0.5	1.7
5% Si	5×10^3	0.22	18	0.5	7
0.1% Si	100	4.3×10^{-3}	918	0.5	349

waves in piezoelectric materials [33,34,66]. Although Si is not piezoelectric, the former bus could be implemented, combining Si with other materials in a layered structure [67]. Another option is to transport the electrons across long QD arrays [29–32].

(3) *Quantum dots.* The characteristic timescales of our protocol depend strongly on the materials used to make the device. Table II summarizes at a glance the typical energy and time scales for different experimental setups. One of the most common materials for QD fabrication is GaAs. All isotopes of both Ga and As have nuclear spin $I = 3/2$ [1]. Since the dwell times are inversely proportional to A_H, the large value $A_H \sim 91.2$ μeV (average value considering the different nuclear isotopes and their natural abundance) [58] in GaAs implies short dwell times of the order of a few to tens of picoseconds. Another well-known material for QD fabrication is Si. Si has two isotopes, but only ^{29}Si is magnetic, with a natural abundance of around 5% and nuclear spin $I = 1/2$. Furthermore, the concentration of ^{29}Si can be controlled by different methods of enrichment. This allows great flexibility in the design of the device, with ensemble sizes ranging from a few nuclei to tens of thousands of them [68–70]. The smaller hyperfine constant $A_H \simeq 4.3$ μeV (for Si with a 100% concentration of ^{29}Si) [41] results in dwell times that can range from a few nanoseconds to a few microseconds depending on the concentration of spinful nuclei.

B. Effect of imperfections

It is important to take into account other effects we have neglected up to now, which lead to nuclear spin decay and decoherence. The T_1 and T_2 times of nuclear spins are long, but finite, and protocols that are slow compared to these times cannot be expected to be well

described by our model (and are thus, likely, not able to produce entanglement). In this regard, the most relevant processes that would hinder the generation of entanglement are nuclear dipole-dipole interactions. In GaAs, nearest-neighbor dipole-dipole interactions are estimated to be about 10^{-5} μeV [1,53], corresponding to $T_{dd} \sim 0.1$ ms. In Si, where the typical distance between nuclei is larger and they have weaker magnetic moment, nearest-neighbor dipole-dipole interactions can be estimated as about 4×10^{-7} μeV (for ^{29}Si at concentrations larger than 12.5%), corresponding to $T_{dd} \sim 1$ ms. Furthermore, reducing the concentration of ^{29}Si would also decrease the strength of these unwanted interactions, leading to longer coherence times for the nuclei. In GaAs QDs, entanglement is generated after tens of microseconds, while one needs hundreds of microseconds for Si devices. The latter result is almost independent of the concentration of ^{29}Si because $T_{ent} \propto N/A_H$. According to these estimations, it seems that reaching the highly entangled transient state is indeed feasible in both GaAs and Si.

Other important factors that affect the performance of our protocol are how well the injected electrons can be prepared in the required initial states and how well they can be transported coherently between the two quantum dots. Imperfect electron spin injection can be modeled considering mixed initial states, i.e.,

$$\xi_{in}^{(n)} = (1-q)\,|s_{in}^{(n)}\rangle\langle s_{in}^{(n)}| + q\sigma^x\,|s_{in}^{(n)}\rangle\langle s_{in}^{(n)}|\,\sigma^x, \quad (16)$$

such that the exact evolution is still given by Eq. (2) with $\chi_{n-1} = \rho_{n-1} \otimes \xi_{in}^{(n)}$, where q corresponds to the spin-flip probability of the injection process ($0 < q < 1$). Dephasing of the electron spin during transport from QD1 to QD2 can be modeled with a dephasing channel acting only on the electronic degrees of freedom, $\mathcal{E}[\rho_{el}] \equiv (1-p)\rho_{el} + p\sigma_z\rho_{el}\sigma_z$. Here p corresponds to the phase-flip probability ($0 \leq p \leq 1$) [71]. The master equation taking into account this imperfection is worked out fully in Appendix A, Eq. (A19). The nonlocal dissipator terms $\mathcal{D}(\mu A_1^+ + \nu A_2^+)$ and $\mathcal{D}(\nu A_1^- + \mu A_2^-)$ are rescaled by a factor $(1-p)$ and additional terms, $p[\mathcal{D}(\mu A_1^+) + \mathcal{D}(\nu A_2^+) + \mathcal{D}(\nu A_1^-) + \mathcal{D}(\mu A_2^-)]/4$, appear. Note that two of these new terms add up to the local polarizing terms already present in the ideal case, whereas the other two constitute new local depolarizing terms. If the strength of these new terms is much smaller than that of the local polarizing terms, $p\mu^2 \ll (\mu - \nu)^2/k$, then the polarizing terms dominate and we expect the nuclear dynamics to be very similar to that in the limit of perfect coherent transport. One could estimate the phase-flip probability from the ensemble-averaged spin dephasing time of the electron spin during transport, which is averaged due to its motion (motional narrowing). The numbers reported in Ref. [66] show that surface-acoustic-wave transport in GaAs itself adds little dephasing, and an estimate of the dephasing

time due to the motionally averaged Overhauser field of the nuclei in the channel suggests a negligible phase-flip probability, $p \sim 1\%$, for a channel of length 5 μm. In Fig. 3, we show the effect of both imperfect electron spin injection and imperfect transport on a small system with two nuclear spins in each ensemble. As can be seen, the protocol still produces an entangled steady state in that case. Further details about the effect of electron spin decoherence during transport and imperfect dwell times are given in Appendix C, where we analyze the homogeneous-system dynamics within the Holstein-Primakoff approximation, using the more general master equation, taking into account those imperfections. The results thus obtained show that even for a phase-flip probability $p \sim 5\%$ it is possible to obtain an entangled steady state (for an homogeneous system) depending on the values of the rest of the parameters.

C. Entanglement detection

One way to measure A_j^z in a gate-defined single QD is to measure electron spin resonance in an external magnetic field B_z, e.g., by determining the resonance frequency at which spin blockade of transport through the QD is lifted [72]. By rotating the nuclear spins using a suitable NMR pulse, the same method can be used to measure $A_j^{x,y}$ (and their variances).

However, there seems to be no direct access to $A_j^{(z,2)}$. One possibility is to exploit the Jaynes-Cummings-like coupling, $H_j^\perp$, of the electron spin to the nuclear ensemble. Neglecting H_j^z for the moment, the probability for an electron spin prepared in the state "down" to flip after a short time $\tau < 1/g_j$ is, to leading order in τ, approximately given by $\tau^2 g_j^2 \langle A_j^+ A_j^- \rangle/4$, and similarly the one for the flip of an initially spin-"up" electron is $\tau^2 g_j^2 \langle A_j^- A_j^+ \rangle/4$. The difference of the two gives $\tau^2 g^2 \langle [A_j^+, A_j^-] \rangle/4 = \tau^2 g^2 \langle A_j^{(z,2)} \rangle/2$. The presence of H_j^z in the hyperfine Hamiltonian leads to corrections of third and higher orders, $-i\tau^3 g^3 \langle [A_j^z, \{A_j^+, A_j^-\}] \rangle/16$, which could be made even smaller if we add an external magnetic field (pointing in the z axis) so as to compensate the Overhauser field $\langle A_j^z \rangle + g\mu_B B_{ext} = 0$. In that case, the correction would be given by $-i\tau^3 g^3 \langle [\delta A_j^z, \{A_j^+, A_j^-\}] \rangle/16$, where $\delta A_j^z \equiv A_j^z - \langle A_j^z \rangle$ is small for the highly polarized states we are considering.

On the other hand, for small ensembles ($N_j < 10$), one may use other techniques, such as those described in Refs. [73,74], that allow single-nucleus addressing.

VI. CONCLUSIONS

In this work we propose a protocol for the deterministic generation of entanglement between two distant ensembles of nuclear spins, which are located around two QDs connected via a coherent electron bus. The protocol relies on the ability to inject electrons with definite polarization in

the QDs and the coherent transfer of the electrons from one QD to the other. Controlling the time the electrons spend trapped in each QD, we engineer a bath that drives the system towards an entangled steady state. The dissipative nature of our protocol makes it inherently robust against imperfections in the dwell times and the electron transport.

Using a bosonization technique, we have fully characterized the steady state in the homogeneous case within the large total angular momentum limit. Furthermore, we have analyzed the dynamics in the inhomogeneous case using the equations of motion for the covariance matrix. There, we have identified two different timescales characterizing the protocol: a faster one related to the collective hyperfine coupling on which the spins are driven into an entangled state, as evidenced by spin squeezing of the collective nuclear spin operators, and a slower one related to the inhomogeneity, which leads to partial dephasing of the entanglement.

While the protocol requires the coherent transport of electron spins—a resource that also allows us to distribute electron spin entanglement—employing the nuclear spins makes an additional resource available for quantum information processing: in a hybrid approach, constantly generated nuclear spin entanglement could be a resource accessed by the electron spin quantum register at need. To take full advantage of the long nuclear coherence time, it would be appealing to store quantum information in the nuclear system, using the electron spins only to operate on the nuclei.

Depending on the chosen experimental implementation of the protocol, the addition of magnetic fields for the measurement of the generated entanglement may not be feasible in sufficiently short times; therefore, an interesting question is whether a simple extension of our protocol would work at finite magnetic field. This is however out of the scope of this work. Note that our protocol generalizes directly to the case of n spin ensembles. This is readily seen in the homogeneous and bosonic limits, where n linearly independent terms akin to the two nonlocal ones in the master equation, Eq. (3), will stabilize an n-mode squeezed vacuum state, which comprise, for example, Gaussian cluster states that allow universal measurement-based quantum computation [75]. Alternatively, pairs of entangled spin ensembles can be merged into multipartite entangled states by performing, for example, a measurement of a joint collective spin component of two of them; combined with full unitary control over the nuclear spins (as conceivable for few or single nuclear spins [24]) this also allows the preparation of computationally universal [76] multipartite entangled states.

APPENDIX A: EFFECTIVE MASTER EQUATION

In the first two steps of the protocol, the nuclear density matrix evolves as

$$\rho_n = \text{tr}_{\text{el}}(e^{-i\tau_2 H_2} \mathcal{E}[e^{-i\tau_1 H_1} \chi_{n-1} e^{i\tau_1 H_1}] e^{i\tau_2 H_2}), \quad \text{(A1)}$$

where the hyperfine interaction Hamiltonian is given by

$$H_j = \frac{g_j}{2}(A_j^+ S_j^- + A_j^- S_j^+) + g_j A_j^z S_j^z, \quad \text{(A2)}$$

and $\mathcal{E}$ is a quantum channel that models the evolution of the electron spin during transfer from QD1 to QD2. To ease notation, we suppress here and in the following the superscript (n) in the dwelling times τ_j (and the injected states $|s_{\text{in}}\rangle$, as it is always clear what step we are talking about). We take it as a phase-flip channel [71, p. 384], with probability $0 \leq p \leq 1$, $\mathcal{E}[\rho_{\text{el}}] = (1-p)\rho_{\text{el}} + p\sigma_z \rho_{\text{el}} \sigma_z$, where the σ_α ($\alpha = x, y, z$) denote the Pauli matrices. Expanding the exponentials up to second order in Eq. (A1), we can approximate

$$\rho_{n+1} \simeq \text{tr}_{\text{el}}\Big(\mathcal{E}[\chi_n] - i\tau_1 \mathcal{E}[[H_1, \chi_n]] - i\tau_2[H_2, \mathcal{E}[\chi_n]]$$

$$- \frac{\tau_1^2}{2}\mathcal{E}[[H_1, [H_1, \chi_n]]] - \frac{\tau_2^2}{2}[H_2, [H_2, \mathcal{E}[\chi_n]]]$$

$$- \tau_1 \tau_2[H_2, \mathcal{E}[[H_1, \chi_n]]] \Big). \quad \text{(A3)}$$

Here, $\text{tr}_{\text{el}}(\cdot)$ denotes the trace over the electronic degrees of freedom. Computing the trace term by term, we have

$$\text{tr}_{\text{el}}(\mathcal{E}[\chi_n]) = \rho_n, \quad \text{(A4)}$$

$$-i\tau_1 \text{tr}_{\text{el}}(\mathcal{E}[[H_1, \chi_n]]) = \mp i\frac{\tau_1 g_1}{2}[A_1^z, \rho_n], \quad \text{(A5)}$$

$$-i\tau_2 \text{tr}_{\text{el}}([H_2, \mathcal{E}[\chi_n]]) = \mp i\frac{\tau_2 g_2}{2}[A_2^z, \rho_n], \quad \text{(A6)}$$

$$-\frac{\tau_1^2}{2}\,\mathrm{tr}_{\mathrm{el}}(\mathcal{E}[[H_1,[H_1,\chi_n]]]) = \frac{\tau_1^2 g_1^2}{4}\{\mathcal{D}(A_1^z)[\rho_n] + \mathcal{D}(A_1^\pm)[\rho_n]\}, \tag{A7}$$

$$-\frac{\tau_2^2}{2}\,\mathrm{tr}_{\mathrm{el}}([H_2,[H_2,\mathcal{E}[\chi_n]]]) = \frac{\tau_2^2 g_2^2}{4}\{\mathcal{D}(A_2^z)[\rho_n] + \mathcal{D}(A_2^\pm)[\rho_n]\}, \tag{A8}$$

$$-\tau_1\tau_2\,\mathrm{tr}_{\mathrm{el}}([H_2,\mathcal{E}[[H_1,\chi_n]]]) = -\frac{\tau_1 g_1 \tau_2 g_2}{4}\{[A_2^z,(A_1^z,\rho_n)] + (1-2p)([A_2^\mp, A_1^\pm \rho_n] - [A_2^\pm, \rho_n A_1^\mp])\}, \tag{A9}$$

where the upper (lower) sign has to be chosen if $|s_{\mathrm{in}}\rangle = |\uparrow\rangle$ ($|s_{\mathrm{in}}\rangle = |\downarrow\rangle$). Note that, since $\mathcal{E}$ is a trace-preserving quantum channel that does not affect fully polarized input states, its presence can be neglected in all the terms except the last, Eq. (A9).

The second-order z terms can be simplified as

$$\frac{\tau_1^2 g_1^2}{4}\mathcal{D}(A_1^z)[\rho_n] + \frac{\tau_2^2 g_2^2}{4}\mathcal{D}(A_2^z)[\rho_n] - \frac{\tau_1 g_1 \tau_2 g_2}{4}[A_2^z,[A_1^z,\rho_n]] = \frac{1}{4}\mathcal{D}(\tau_1 g_1 A_1^z + \tau_2 g_2 A_2^z)[\rho_n], \tag{A10}$$

while the $\pm$ terms can be rewritten as

$$\frac{\tau_1^2 g_1^2}{4}\mathcal{D}(A_1^\pm)[\rho_n] + \frac{\tau_2^2 g_2^2}{4}\mathcal{D}(A_2^\pm)[\rho_n] - \frac{\tau_1 g_1 \tau_2 g_2(1-2p)}{4}([A_2^\mp, A_1^\pm \rho_n] - [A_2^\pm, \rho_n A_1^\mp])$$
$$= \frac{1-2p}{4}\mathcal{D}(\tau_1 g_1 A_1^\pm + \tau_2 g_2 A_2^\pm)[\rho_n] \mp \frac{\tau_1 g_1 \tau_2 g_2(1-2p)}{8}([A_2^- A_1^+, \rho_n] + [\rho_n, A_1^- A_2^+])$$
$$+ \frac{\tau_1^2 g_1^2 p}{2}\mathcal{D}(A_1^\pm)[\rho_n] + \frac{\tau_2^2 g_2^2 p}{2}\mathcal{D}(A_2^\pm)[\rho_n]. \tag{A11}$$

Thus, after the first step of the protocol, the nuclei's reduced density matrix evolves as

$$\rho_{n+1} \simeq \rho_n - \frac{i}{2}[\mu_1 A_1^z + \nu_2 A_2^z, \rho_n] + \frac{1}{4}\mathcal{D}(\mu_1 A_1^z + \nu_2 A_2^z)[\rho_n] + \frac{1-2p}{4}\mathcal{D}(\mu_1 A_1^+ + \nu_2 A_2^+)[\rho_n]$$
$$- \frac{\mu_1 \nu_2(1-2p)}{8}([A_2^- A_1^+, \rho_n] + [\rho_n, A_1^- A_2^+]) + \frac{\mu_1^2 p}{2}\mathcal{D}(A_1^+)[\rho_n] + \frac{\nu_2^2 p}{2}\mathcal{D}(A_2^+)[\rho_n], \tag{A12}$$

while after the second step, the nuclei's reduced density matrix evolves as

$$\rho_{n+2} \simeq \rho_{n+1} + \frac{i}{2}[\nu_1 A_1^z + \mu_2 A_2^z, \rho_{n+1}] + \frac{1}{4}\mathcal{D}(\nu_1 A_1^z + \mu_2 A_2^z)[\rho_{n+1}] + \frac{1-2p}{4}\mathcal{D}(\nu_1 A_1^- + \mu_2 A_2^-)[\rho_{n+1}]$$
$$+ \frac{\nu_1 \mu_2(1-2p)}{8}([A_2^- A_1^+, \rho_{n+1}] + [\rho_{n+1}, A_1^- A_2^+]) + \frac{\nu_1^2 p}{2}\mathcal{D}(A_1^-)[\rho_{n+1}] + \frac{\mu_2^2 p}{2}\mathcal{D}(A_2^-)[\rho_{n+1}]. \tag{A13}$$

The concatenation of these two steps yields

$$\rho_{n+2} \simeq \rho_n + \frac{i}{2}[(\nu_1 - \mu_1)A_1^z + (\mu_2 - \nu_2)A_2^z, \rho_n] + \frac{1}{4}\mathcal{D}((\nu_1 - \mu_1)A_1^z + (\mu_2 - \nu_2)A_2^z)[\rho_n]$$
$$+ \frac{1-2p}{4}\mathcal{D}(\nu_1 A_1^- + \mu_2 A_2^-)[\rho_n] + \frac{1-2p}{4}\mathcal{D}(\mu_1 A_1^+ + \nu_2 A_2^+)[\rho_n]$$
$$+ \frac{\nu_1^2 p}{2}\mathcal{D}(A_1^-)[\rho_n] + \frac{\mu_2^2 p}{2}\mathcal{D}(A_2^-)[\rho_n] + \frac{\mu_1^2 p}{2}\mathcal{D}(A_1^+)[\rho_n] + \frac{\nu_2^2 p}{2}\mathcal{D}(A_2^+)[\rho_n]$$
$$+ \frac{(\mu_2 \nu_1 - \mu_1 \nu_2)(1-2p)}{8}([A_2^- A_1^+, \rho_n] + [\rho_n, A_1^- A_2^+]). \tag{A14}$$

For the second part, we first work out the concatenation of m steps with $|s_{\mathrm{in}}\rangle = |\downarrow\rangle$, $\tau_1 g_1 = (\mu_1 - \nu_1)/k$, and $\tau_2 g_2 = 0$. Up to second order we find that

$$\rho_{n+2+m} \simeq \rho_{n+2} + \frac{i(\mu_1 - \nu_1)}{2k}c_m[A_1^z, \rho_{n+2}] + \frac{(\mu_1 - \nu_1)^2}{4k^2}d_m\mathcal{D}(A_1^z)[\rho_{n+2}] + \frac{(\mu_1 - \nu_1)^2}{4k^2}c_m\mathcal{D}(A_1^-)[\rho_{n+2}], \tag{A15}$$

where the coefficients obey a simple recurrence relation $c_m = c_{m-1} + 1$ and $d_m = d_{m-1} + 1 + 2c_{m-1}$ for $m > 1$, and $c_1 = d_1 = 1$. Therefore, the concatenation of k such steps leads to

$$\rho_{n+2+k} \simeq \rho_{n+2} + \frac{i(\mu_1 - \nu_1)}{2}[A_1^z, \rho_{n+2}] + \frac{(\mu_1 - \nu_1)^2}{4}\mathcal{D}(A_1^z)[\rho_{n+2}] + \frac{(\mu_1 - \nu_1)^2}{4k}\mathcal{D}(A_1^-)[\rho_{n+2}]. \tag{A16}$$

Similarly, the concatenation of k steps with $|s_{in}\rangle = |\uparrow\rangle$, $\tau_1 g_1 = 0$, and $\tau_2 g_2 = (\mu_2 - \nu_2)/k$ produces

$$\rho_{n+2+2k} \simeq \rho_{n+2+k} - \frac{i(\mu_2 - \nu_2)}{2}[A_2^z, \rho_{n+2+k}] + \frac{(\mu_2 - \nu_2)^2}{4}\mathcal{D}(A_2^z)[\rho_{n+2+k}] + \frac{(\mu_2 - \nu_2)^2}{4k}\mathcal{D}(A_2^+)[\rho_{n+2+k}]. \tag{A17}$$

Thus, the concatenation of k steps of the first kind, followed by k steps of the second kind results in

$$\rho_{n+2+2k} \simeq \rho_{n+2} - \frac{i}{2}[(\nu_1 - \mu_1)A_1^z + (\mu_2 - \nu_2)A_2^z, \rho_{n+2}] + \frac{1}{4}\mathcal{D}((\nu_1 - \mu_1)A_1^z + (\mu_2 - \nu_2)A_2^z)[\rho_{n+2}]$$
$$+ \frac{(\mu_2 - \nu_2)^2}{4k}\mathcal{D}(A_2^+)[\rho_{n+2}] + \frac{(\mu_1 - \nu_1)^2}{4k}\mathcal{D}(A_1^-)[\rho_{n+2}]. \tag{A18}$$

Last, putting together the equations for the first and second parts of the protocol, all z terms cancel and we get

$$\Delta\rho_n \simeq \frac{1 - 2p}{4}\mathcal{D}(\nu_1 A_1^- + \mu_2 A_2^-)[\rho_n] + \frac{1 - 2p}{4}\mathcal{D}(\mu_1 A_1^+ + \nu_2 A_2^+)[\rho_n]$$
$$+ \left[\frac{(\mu_1 - \nu_1)^2}{4k} + \frac{\nu_1^2 p}{2}\right]\mathcal{D}(A_1^-)[\rho_n] + \left[\frac{(\mu_2 - \nu_2)^2}{4k} + \frac{\nu_2^2 p}{2}\right]\mathcal{D}(A_2^+)[\rho_n]$$
$$+ \frac{\mu_2^2 p}{2}\mathcal{D}(A_2^-)[\rho_n] + \frac{\mu_1^2 p}{2}\mathcal{D}(A_1^+)[\rho_n] + \frac{(\mu_2\nu_1 - \mu_1\nu_2)(1 - 2p)}{8}([A_2^- A_1^+, \rho_n] + [\rho_n, A_1^- A_2^+]), \tag{A19}$$

where we have defined $\Delta\rho_n \equiv \rho_{n+2+2k} - \rho_n$.

APPENDIX B: FIDELITIES FOR HOMOGENEOUS SYSTEMS

In Fig. 5, we show the fidelity of the steady state with respect to the two-mode spin squeezed state [Eq. (7) in the main text] as a function of the number of steps in the cycle. The system consists of two identical homogeneous ensembles of spin-1/2 nuclei. The initial state belongs to the subspace with maximal total angular momenta $J_j = N_j/2$. As expected, the fidelity increases for increasing k.

For small systems with $N_j < 10$, the EPR uncertainty may not detect entanglement if k is too small; see Fig. 6(a). Of course, making k larger brings Δ_{EPR} closer to the value in the ideal state, which does show entanglement irrespective of the number of nuclei considered. Nonetheless, according to the PPT criterion [62] the system is indeed entangled for all values of k and N; see Fig. 6(b). But, how can this entanglement be detected experimentally? An entanglement witness for the simplest case of just two qubits ($N_1 = N_2 = 1$, $I = 1/2$) can be constructed based on the following inequality, valid for separable states [48]:

$$p_S \leq \frac{1 - m^2}{2}. \tag{B1}$$

Here, $\mathbf{m} \equiv \langle \mathbf{J} \rangle$ ($m \equiv \|\mathbf{m}\|$) is the expected value of the total spin, where in this case $\mathbf{J} = \mathbf{I}_{11} + \mathbf{I}_{12}$, and $p_S \equiv \langle \Psi_- | \rho | \Psi_- \rangle$ is the singlet occupation. Since $(1 - m^2) \leq 1$,
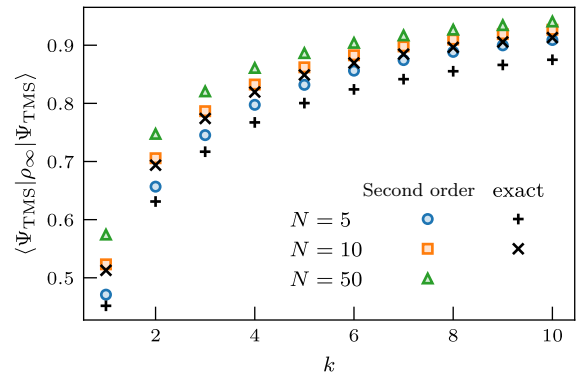

FIG. 5. Fidelity of the steady state with respect to the two-mode spin squeezed state for an homogeneous system of spin-1/2 nuclei as a function of the number of repetitions k performed in the last two steps of the protocol. The parameters of the system are $N_1 = N_2 = N$, $\mu = 0.5/\sqrt{N}$, and $\nu = 0.8\mu$. The steady state has been computed using the approximate second-order master equation, Eq. (3) in the main text, and also using the exact time evolution superoperator, Eq. (2) in the main text.
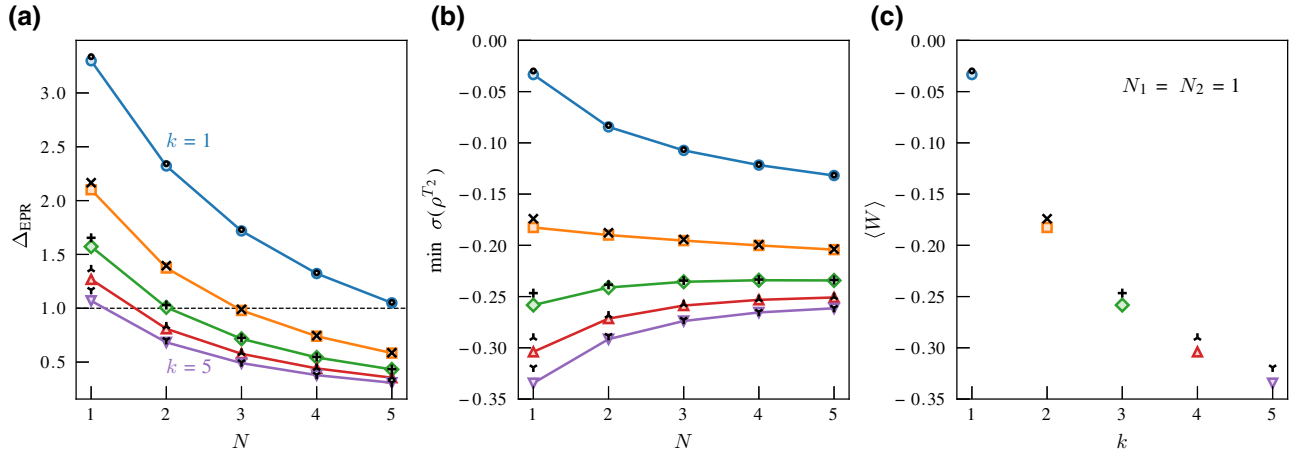
FIG. 6. EPR uncertainty (a), minimum eigenvalue of the partial transpose (b), and entanglement witness based on the singlet occupation (c), for the steady state of a homogeneous system of spin-1/2 nuclei with parameters $N_1 = N_2 = N$, $\mu = 0.1/\sqrt{N}$, and $\nu = 0.8\mu$. For small k and N, the EPR criterion fails to detect entanglement, although the negativity of the partial transpose shows that the system is indeed entangled. The steady state has been computed using the approximate second-order master equation (filled symbols), Eq. (3) in the main text, and also using the exact time evolution superoperator (black symbols), Eq. (2) in the main text.

then $p_S > 1/2$ implies that the two spins are entangled. Thus, we define the entanglement witness

$$W = \tfrac{1}{2} - |\Psi_-\rangle\langle\Psi_-| = \tfrac{1}{2}(\mathbf{J}^2 - 1) = \tfrac{1}{4} + \mathbf{I}_{11} \cdot \mathbf{I}_{12} \quad \text{(B2)}$$

such that $\langle W \rangle < 0$ for entangled states. In Fig. 6(c) we indeed show that this entanglement witness is able to detect the entanglement produced by our protocol.

APPENDIX C: HOLSTEIN-PRIMAKOFF TRANSFORMATION

In the limit of large total angular momenta and large polarizations, we can study the nuclear dynamics analytically, replacing the collective total angular momentum operators by bosonic operators, $A_1^- \to \sqrt{r_1}a_1^\dagger$ ($A_1^+ \to \sqrt{r_1}a_1$) and $A_2^+ \to \sqrt{r_2}a_2^\dagger$ ($A_2^- \to \sqrt{r_2}a_2$) in Eq. (A19). Doing so, defining $\tilde{\mu}_j \equiv \mu_j \sqrt{r_j}$ and $\tilde{\nu}_j \equiv \nu_j \sqrt{r_j}$, we obtain the master equation

$$\Delta\rho_n \simeq \frac{1-2p}{4}\mathcal{D}(\tilde{\nu}_1 a_1^\dagger + \tilde{\mu}_2 a_2)[\rho_n]$$

$$+ \frac{1-2p}{4}\mathcal{D}(\tilde{\mu}_1 a_1 + \tilde{\nu}_2 a_2^\dagger)[\rho_n]$$

$$+ \left[\frac{(\tilde{\mu}_1 - \tilde{\nu}_1)^2}{4k} + \frac{\tilde{\nu}_1^2 p}{2}\right]\mathcal{D}(a_1^\dagger)[\rho_n]$$

$$+ \left[\frac{(\tilde{\mu}_2 - \tilde{\nu}_2)^2}{4k} + \frac{\tilde{\nu}_2^2 p}{2}\right]\mathcal{D}(a_2^\dagger)[\rho_n]$$

$$+ \frac{\tilde{\mu}_2^2 p}{2}\mathcal{D}(a_2)[\rho_n] + \frac{\tilde{\mu}_1^2 p}{2}\mathcal{D}(a_1)[\rho_n]$$

$$+ \frac{(\tilde{\mu}_2\tilde{\nu}_1 - \tilde{\mu}_1\tilde{\nu}_2)(1-2p)}{8}([a_2 a_1, \rho_n] + [\rho_n, a_1^\dagger a_2^\dagger]). \quad \text{(C1)}$$

From this master equation, using the identities

$$\text{tr}\{B[A,\rho]\} = \langle[B,A]\rangle, \quad \text{(C2)}$$

$$\text{tr}\{B\mathcal{D}(A)[\rho]\} = \tfrac{1}{2}\langle[A^\dagger, B]A + A^\dagger[B,A]\rangle, \quad \text{(C3)}$$

one can obtain the equation of motion of any operator expressed in terms of $\{a_j, a_j^\dagger\}_{j=1,2}$. Because of the bosonic commutation relations, the equation of motion of any product of these bosonic operators will depend only on products of the same or lower order. Hence, to find the steady-state expectation value of any set of monomials in these bosonic variables, we just have to solve a finite linear system of equations. We are interested in computing the EPR uncertainty, which depends on the absolute value polarizations $|\langle J_j^z \rangle| \simeq J_j - \langle a_j^\dagger a_j \rangle$ and variances

$$\text{var}(J_1^{x/y} + J_2^{x/y}) \simeq \frac{J_1 + J_2}{2} \pm \frac{J_1}{2}\langle a_1^\dagger a_1^\dagger \pm 2a_1^\dagger a_1 + a_1 a_1\rangle$$

$$\pm \frac{J_2}{2}\langle a_2^\dagger a_2^\dagger \pm 2a_2^\dagger a_2 + a_2 a_2\rangle$$

$$+ \sqrt{J_1 J_2}\langle a_1^\dagger a_2^\dagger \pm a_1^\dagger a_2 \pm a_2^\dagger a_1 + a_1 a_2\rangle$$

$$\mp \left(\sqrt{\frac{J_1}{2}}\langle a_1^\dagger \pm a_1\rangle \pm \sqrt{\frac{J_2}{2}}\langle a_2^\dagger \pm a_2\rangle\right)^2. \quad \text{(C4)}$$

Thus, we have to compute the steady-state expectation values of all monomials up to second order. Their equations of motion are

$$\Delta \langle a_j \rangle = \kappa_j \langle a_j \rangle + \delta_{j,2} \epsilon \langle a_1^\dagger \rangle, \tag{C5}$$

$$\Delta \langle a_j^2 \rangle = 2\kappa_j \langle a_j^2 \rangle + \delta_{j,2} 2\epsilon \langle a_1^\dagger a_2 \rangle, \tag{C6}$$

$$\Delta \langle a_j^\dagger a_j \rangle = 2\kappa_j \langle a_j^\dagger a_j \rangle + 2\kappa_j + \frac{\tilde{\mu}_j^2}{4} + \delta_{j,2} \epsilon \langle a_1^\dagger a_2^\dagger + a_1 a_2 \rangle, \tag{C7}$$

$$\Delta \langle a_1 a_2 \rangle = (\kappa_1 + \kappa_2) \langle a_1 a_2 \rangle + \epsilon \langle a_1^\dagger a_1 \rangle - \frac{(1-2p)\tilde{\mu}_2 \tilde{\nu}_1}{4}, \tag{C8}$$

$$\Delta \langle a_1^\dagger a_2 \rangle = (\kappa_1 + \kappa_2) \langle a_1^\dagger a_2 \rangle + \epsilon \langle a_1^\dagger a_1^\dagger \rangle, \tag{C9}$$

where we have defined

$$\kappa_j = \frac{(\tilde{\nu}_j - \tilde{\mu}_j)}{8} \left[\tilde{\nu}_j + \tilde{\mu}_j + \frac{(\tilde{\nu}_j - \tilde{\mu}_j)}{k} \right],$$

$$\epsilon = \frac{(1-2p)(\tilde{\mu}_1 \tilde{\nu}_2 - \tilde{\mu}_2 \tilde{\nu}_1)}{4}. \tag{C10}$$

The adjoint operators evolve according to $\Delta X^\dagger = (\Delta X)^\dagger$. By definition, the steady-state expectation value of an operator X, $\langle X \rangle_\infty$, satisfies $\Delta \langle X \rangle_\infty = 0$. For the operators we are considering, the only nonzero expectation values turn out to be

$$\langle a_1^\dagger a_1 \rangle_\infty = -1 - \frac{\tilde{\mu}_1^2}{8\kappa_1}, \tag{C11}$$

$$\langle a_1 a_2 \rangle_\infty = \langle a_1^\dagger a_2^\dagger \rangle_\infty = \frac{1}{\kappa_1 + \kappa_2}$$
$$\times \left[\epsilon \left(1 + \frac{\tilde{\mu}_1^2}{8\kappa_1} \right) + \frac{(1-2p)\tilde{\mu}_2 \tilde{\nu}_1}{4} \right], \tag{C12}$$

$$\langle a_2^\dagger a_2 \rangle_\infty = -1 - \frac{\tilde{\mu}_2^2}{8\kappa_2} - \frac{\epsilon}{\kappa_2(\kappa_1 + \kappa_2)}$$
$$\times \left[\epsilon \left(1 + \frac{\tilde{\mu}_1^2}{8\kappa_1} \right) + \frac{(1-2p)\tilde{\mu}_2 \tilde{\nu}_1}{4} \right]. \tag{C13}$$

Since many of the expectation values vanish, the formulas for the variances can be simplified as

$$\text{var}(J_1^x + J_2^x)_\infty = \text{var}(J_1^y + J_2^y)_\infty = \frac{J_1 + J_2}{2} + J_1 \langle a_1^\dagger a_1 \rangle$$
$$+ J_2 \langle a_2^\dagger a_2 \rangle + 2\sqrt{J_1 J_2} \langle a_1 a_2 \rangle. \tag{C14}$$

Substituting these back into the formulas for $|\langle J_j^z \rangle|$ and $\text{var}(J_1^{x/y} + J_2^{x/y})$, we can obtain an analytical expression for Δ_{EPR} in the steady state. In Eq. (11) of the main text we show the analytical formula obtained for Δ_{EPR} in the case of an ideal protocol ($p = 0$, $\mu_1 = \mu_2 = \mu$, and $\nu_1 = \nu_2 = $

ν). In Fig. 7 we show the values of Δ_{EPR} as a function of various parameters [cf. Fig. 2(a) of the main text]. In light of this we conclude that, at least for homogeneous ensembles, the protocol is able to produce entanglement for a wide range of values of the dwell times. These results also demonstrate that the protocol is robust against a certain amount of decoherence during electron transport.

Moreover, from the corresponding equations of motion, we can obtain the evolution of the expected number of bosons in each mode (and, therefore, the polarization of each ensemble). For an ideal protocol, they are given by

$$\langle a_j^\dagger a_j \rangle_n = (1 - 2\kappa r_j)^n \left(\langle a_j^\dagger a_j \rangle_0 + \frac{\kappa - \eta}{2\kappa} \right) - \frac{\kappa - \eta}{2\kappa}, \tag{C15}$$

where we have defined $\kappa \equiv (\mu\nu - \nu^2)/4$ and $\eta \equiv \mu^2/4 - \kappa$. From these equations, we can deduce an analytical expression for the stabilization time:

$$T = -\frac{1}{\log(1 - 2\kappa r_j)} \simeq \frac{1}{2\kappa r_j}. \tag{C16}$$

In Fig. 8, we present results for the stabilization times of homogeneous systems. We show that this time depends on the initial state chosen, and for the fully polarized initial state $|\Psi_{\text{FP}}\rangle = |\Uparrow\rangle_1 |\Downarrow\rangle_2$, it follows the prediction of the HP approximation.

1. Mixed initial state

In Fig. 2(c) we consider a product initial state $\rho_0 = \rho_{\text{QD1}} \otimes \rho_{\text{QD2}}$, where the initial state of each ensemble is mixed, $\rho_{\text{QD}j} = \sum_J p_j(J)\rho_j(J)$. Here, $\rho_j(J)$ is a normalized density matrix that belongs to the jth-ensemble subspace of states with total angular momentum J. Normalization of ρ_0 requires $\sum_J p_j(J) = 1$. As explained in the main text, for homogeneous systems, the steady state will be given by $\rho_\infty = \sum_{J_1,J_2} p_1(J_1)p_2(J_2)\rho_\infty(J_1, J_2)$, with $\rho_\infty(J_1, J_2)$ some steady state within the (J_1, J_2) subspace (the steady state is unique up to variations of the permutation quantum numbers). It can be computed numerically as the kernel of the Liouvillian corresponding to the evolution prescribed by Eq. (2) or the master equation, Eq. (3), or analytically using the HP transformation. However, this latter approach would only yield a good approximation if the initial distributions $p_j(J)$ are peaked towards higher angular momenta.

In this manuscript we consider two different kinds of total angular momentum distributions. On the one hand, we consider an equal-weight mixture of all states with angular momenta $J_j \geq J_j^{\text{min}}$. In this case the probabilities
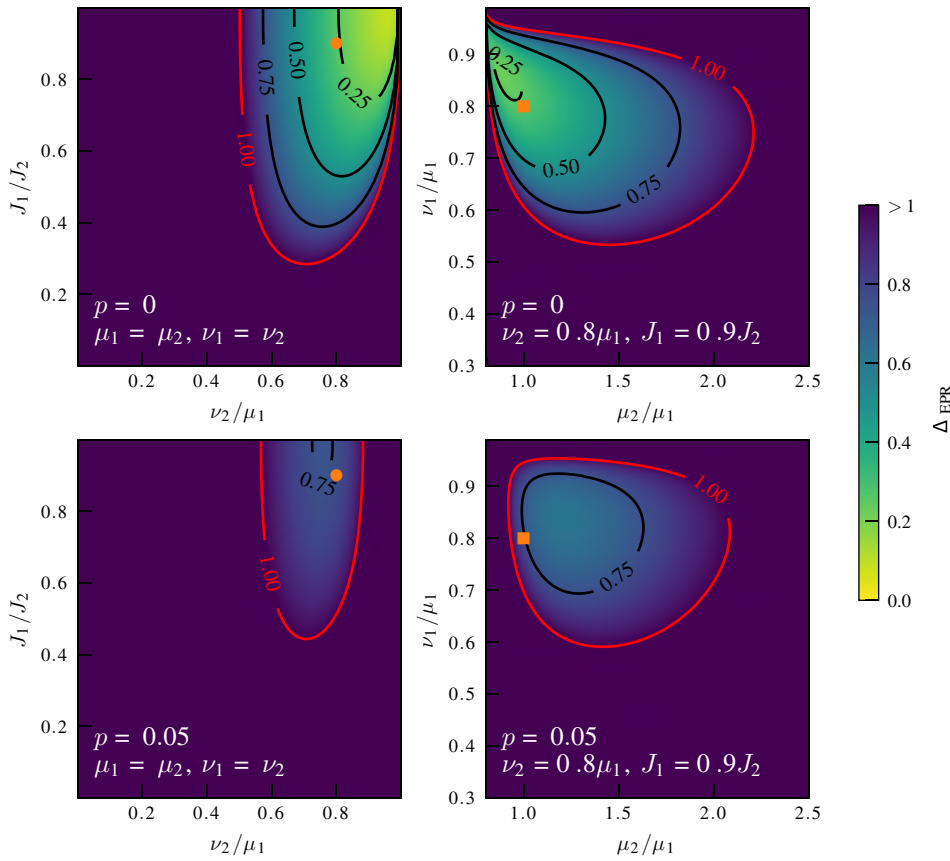
FIG. 7. Dependence of the EPR uncertainty as given by the HP approximation on various parameters. In all the plots shown, $k = 1$, $r_1 = 0.9$, and $r_2 = 0.8$. Other fixed parameters have the values indicated in each plot. The orange dots in the panels of the left column correspond to the fixed values of N_1/N_2 and ν_2/μ_1 used in the other two panels. The orange squares in the panels of the right column correspond to the "ideal" choice $\mu_1 = \mu_2$ and $\nu_1 = \nu_2$.

$p_j(J)$ are given, up to a normalization constant, by

$$p_j(J) \propto \begin{cases} (2J+1)D_j(J) & \text{for } J \geq J_j^{\min}, \\ 0 & \text{for } J < J_j^{\min}, \end{cases} \quad \text{(C17)}$$

where

$$D_j(J) = \binom{N_j}{N_j/2 - J} - \binom{N_j}{N_j/2 - J - 1} \quad \text{(C18)}$$

corresponds to the degeneracy of the Dicke states for non-maximal total angular momentum J. Since the number of states with total angular momentum J increases as J decreases, this probability distribution is peaked at $J_j^{\min}$ and decays towards higher values of J. On the other hand, we have considered Gaussian distributions with mean
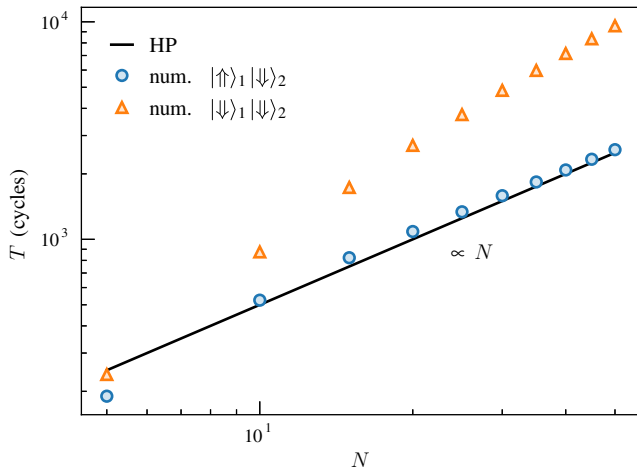

FIG. 8. Stabilization time as a function of the number of nuclei considered, $N_1 = N_2 = N$, for an ideal protocol with parameters $\mu = 0.5/\sqrt{N}$ and $\nu = 0.8\mu$, performed in an homogeneous system of spin-1/2 nuclei. Filled symbols correspond to the numerically obtained stabilization times for two different initial states, whereas the line corresponds to the formula $T = 1/(2\kappa)$.
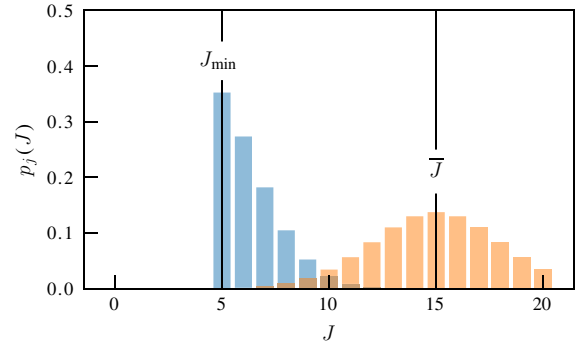

FIG. 9. Equal-weight mixture distribution (blue bars) and Gaussian distribution with variance $w^2 = 3.0$ (orange bars) for an ensemble with $N = 40$ spin-1/2 nuclei.

value $\bar{J}$ and variance w^2,

$$p_j(J) \propto \exp\left(-\frac{(J-\bar{J})^2}{2w^2}\right). \tag{C19}$$

In Fig. 9, we compare both kinds of distribution.

APPENDIX D: NONLINEAR EQUATIONS OF MOTION

In this section we show how to obtain the equations of motion, and asses the validity of several different approximation schemes to close them. From the second-order master equation, Eq. (3) in the main text, using the identity $\mathrm{tr}(B\mathcal{D}(A)[\rho]) = \langle [A^\dagger, B]A + A^\dagger[B, A]\rangle/2$, we obtain the following general equations of motion, valid for any operator X:

$$\begin{aligned}
\Delta\langle X\rangle &= \frac{\mu^2}{8}\sum_{j=1,2}\langle[[A_j^-, X], A_j^+] + [A_j^-, [X, A_j^+]]\rangle \\
&+ \frac{\mu\nu}{8}\sum_{j=1,2}\langle[[A_j^-, X], A_{3-j}^+] + [A_j^-, [X, A_{3-j}^+]]\rangle \\
&+ \frac{\nu^2 - \mu\nu}{4}\langle[A_1^+, X]A_1^- + A_1^+[X, A_1^-] \\
&+ [A_2^-, X]A_2^+ + A_2^-[X, A_2^+]\rangle.
\end{aligned} \tag{D1}$$

Substituting X by $\sigma_{ij}^+\sigma_{i'j'}^-$ and $\sigma_{ij}^z\sigma_{i'j'}^z$, we obtain the equations of motion presented in the main text, Eqs. (12) and (13). However, these equations are quite involved and do not allow a clear vision of the evolution of the system. For this, we instead first investigate the polarization dynamics in each ensemble separately, and then investigate the dynamics of the transverse spin variance.

1. Polarization dynamics

From the second-order master equation, we find the general equation of motion

$$\begin{aligned}
\Delta\langle X_1\rangle &= \frac{\eta - \kappa}{2}\langle[A_1^+, X_1]A_1^- + A_1^+[X_1, A_1^-]\rangle \\
&+ \frac{\eta + \kappa}{2}\langle[A_1^-, X_1]A_1^+ + A_1^-[X_1, A_1^+]\rangle,
\end{aligned} \tag{D2}$$

valid for any operator X_1 that acts nontrivially only on the nuclei belonging to the first ensemble. For an operator X_2 that acts nontrivially only on the nuclei belonging to the second ensemble, we obtain the same equation, replacing $A_1^\pm \to A_2^\mp$, or, equivalently, changing $\kappa \to -\kappa$ and the subindex $1 \to 2$.

We can realize that if the coupling constants $\{g_{i2}\}$ and $\{g_{i1}\}$ are the same, that is, if the two ensembles are identical, the steady-state polarization of the second ensemble

must be the same as that of the first, but with opposite sign. This can be seen by applying a transformation $U = \prod_i \sigma_{i2}^x$, which transforms $A_2^\pm \to \tilde{A}_2^\mp$, $J_2^z \to -\tilde{J}_2^z$. Thus, the equation of motion for $\langle\tilde{J}_2^z\rangle$ would be the same as that for $\langle J_1^z\rangle$ (also with the same initial value if the initial state is $|\Uparrow\rangle_1|\Downarrow\rangle_2$). Undoing the transformation, the steady-state polarization in QD2 is $\langle J_2^z\rangle_\infty = -\langle\tilde{J}_2^z\rangle_\infty = -\langle J_1^z\rangle_\infty$.

To compute the polarization of the first ensemble, we particularize Eq. (D2) for $X_1 = \sigma_{i1}^z$ ($i = 1, \ldots, N_1$), obtaining

$$\begin{aligned}
\Delta\langle\sigma_i^z\rangle &= (\kappa - \eta)\sum_k g_k g_i(\langle\sigma_i^+\sigma_k^-\rangle + \langle\sigma_k^+\sigma_i^-\rangle) \\
&+ (\kappa + \eta)\sum_k g_k g_i(\langle\sigma_i^-\sigma_k^+\rangle + \langle\sigma_k^-\sigma_i^+\rangle). \tag{D3}
\end{aligned}$$

Here, and in the following equations, we have dropped the QD index to avoid cluttering. It should be understood that all operators and coupling constants refer to the first ensemble. As it turns out, the individual polarizations depend on all the matrix elements of the covariance matrix $\gamma_{ij} \equiv \langle\sigma_i^+\sigma_j^-\rangle$, which, in turn, depend on higher-order correlations as

$$\begin{aligned}
\Delta\gamma_{ij} &= \frac{\eta - \kappa}{2}\sum_k g_k(g_j\langle\sigma_i^+[\sigma_j^+, \sigma_j^-]\sigma_k^-\rangle \\
&+ g_i\langle\sigma_k^+[\sigma_i^+, \sigma_i^-]\sigma_j^-\rangle) \\
&+ \frac{\eta + \kappa}{2}\sum_k g_k(g_i\langle[\sigma_i^-, \sigma_i^+]\sigma_j^-\sigma_k^+\rangle \\
&+ g_j\langle\sigma_k^-\sigma_i^+[\sigma_j^-, \sigma_j^+]\rangle) \\
&= \frac{\eta - \kappa}{2}\sum_k g_k(g_j\langle\sigma_i^+\sigma_j^z\sigma_k^-\rangle + g_i\langle\sigma_k^+\sigma_i^z\sigma_j^-\rangle) \\
&- \frac{\eta + \kappa}{2}\sum_k g_k(g_i\langle\sigma_i^z\sigma_j^-\sigma_k^+\rangle + g_j\langle\sigma_k^-\sigma_i^+\sigma_j^z\rangle). \tag{D4}
\end{aligned}$$

Rewriting the terms in the second sum as those in the first, we obtain

$$\begin{aligned}
\Delta\gamma_{ij} &= -\kappa\sum_k g_k(g_j\langle\sigma_i^+\sigma_j^z\sigma_k^-\rangle + g_i\langle\sigma_k^+\sigma_i^z\sigma_j^-\rangle) \\
&- (\kappa + \eta)[(g_i^2 + g_j^2)\gamma_{ij} - g_i g_j\lambda_{ij}], \tag{D5}
\end{aligned}$$

where $\lambda_{ij} = \langle\sigma_i^z\sigma_j^z\rangle$. Note that higher-order correlations can be simplified in the case that some indices repeat:

$$\sigma_i^+\sigma_j^z\sigma_k^- = \begin{cases} -\sigma_i^+\sigma_k^- & \text{if } i = j \text{ or } j = k, \\ (\sigma_j^z + \sigma_i^z\sigma_j^z)/2 & \text{if } i = k \neq j. \end{cases} \tag{D6}$$

Therefore,

$$\Delta\gamma_{ii} = \kappa \sum_{k \neq i} g_k g_i (\gamma_{ik} + \gamma_{ki}) - 2\eta g_i^2 \gamma_{ii} + (\kappa + \eta)g_i^2,$$
(D7)

$$\Delta\gamma_{ij} = -\kappa \sum_{k \neq i,j} g_k (g_j \langle \sigma_i^+ \sigma_j^z \sigma_k^- \rangle + g_i \langle \sigma_k^+ \sigma_i^z \sigma_j^- \rangle)$$
$$- \eta(g_i^2 + g_j^2)\gamma_{ij} + \eta g_i g_j \lambda_{ij}$$
$$+ -\kappa g_i g_j (\gamma_{ii} + \gamma_{jj} - 1) \quad \text{for } i \neq j.$$
(D8)

The equations of motion for the zz correlations can be obtained in an analogous way:

$$\Delta\lambda_{ij} = 2\kappa \sum_{k \neq i,j} g_k [g_j (\langle \sigma_j^+ \sigma_i^z \sigma_k^- \rangle + \langle \sigma_k^+ \sigma_i^z \sigma_j^- \rangle)$$
$$+ g_i (\langle \sigma_i^+ \sigma_j^z \sigma_k^- \rangle + \langle \sigma_k^+ \sigma_j^z \sigma_i^- \rangle)]$$
$$+ 4\eta g_i g_j (\gamma_{ij} + \gamma_{ji}) - 2\eta(g_i^2 + g_j^2)\lambda_{ij}$$
$$+ 2\kappa [g_i^2 (2\gamma_{jj} - 1) + g_j^2 (2\gamma_{ii} - 1)] \quad \text{for } i \neq j.$$
(D9)

For the nuclei in the second ensemble, we obtain equations similar to those presented so far, the only difference being the change of sign $\kappa \rightarrow -\kappa$.

The different approximation schemes that we have considered are as follows [52].

(1) *Spin temperature.* Neglecting all correlations $\langle \sigma_i^+ \sigma_j^- \rangle \approx 0$ for $i \neq j$, Eq. (D3) leads to an independent equation of motion for each nucleus,

$$\Delta\langle \sigma_i^z \rangle = -2\eta g_i^2 \langle \sigma_i^z \rangle + 2\kappa g_i^2.$$
(D10)

(2) *Boson.* Deviations from the fully polarized state can be approximated as bosonic excitations. Substituting spin operators by bosonic operators, $\sigma_i^- \rightarrow a_i^\dagger$ and $\sigma_i^z \rightarrow 1 - 2a_i^\dagger a_i$, for the nuclei in the first ensemble, we can approximate $[\sigma_i^+, \sigma_j^-] \approx \delta_{ij}$ in Eq. (D4), obtaining a closed set of equations:

$$\Delta\gamma_{ij} = -\kappa \sum_k g_k (g_j \gamma_{ik} + g_i \gamma_{kj}) + (\eta + \kappa)g_i g_j. \quad \text{(D11)}$$

Note that within this approximation the polarization of each nucleus in the first ensemble should be computed as $\langle \sigma_i^z \rangle = 3 - 2\gamma_{ii}$. For the second ensemble, we substitute $\sigma_i^- \rightarrow a_i$ and $\sigma_i^z \rightarrow 2a_i^\dagger a_i - 1$ ($[\sigma_i^+, \sigma_j^-] \approx -\delta_{ij}$), obtaining

$$\Delta\gamma_{ij} = -\kappa \sum_k g_k (g_j \gamma_{ik} + g_i \gamma_{kj}) + (\eta - \kappa)g_i g_j. \quad \text{(D12)}$$

The polarization of the nuclei in the second ensemble can be computed using the usual formula $\langle \sigma_i^z \rangle = 2\gamma_{ii} - 1$.

For the rest of schemes, we use Eqs. (D7) and (D8), approximating

(3) *Hartree:* $\langle \sigma_i^+ \sigma_j^z \sigma_k^- \rangle \approx (2\gamma_{jj} - 1)\gamma_{ik}$;
(4) *Wick:* $\langle \sigma_i^+ \sigma_j^z \sigma_k^- \rangle \approx (2\gamma_{jj} - 1)\gamma_{ik} + 2\gamma_{ij}\gamma_{jk}$;
(5) *Spin:* $\langle \sigma_i^+ \sigma_j^z \sigma_k^- \rangle \approx (2\gamma_{jj} - 1)\gamma_{ik} - 2\gamma_{ij}\gamma_{jk}$.

We may approximate as well the zz correlations $\langle \sigma_i^z \sigma_j^z \rangle = 2\langle \sigma_i^+ \sigma_j^z \sigma_i^- \rangle - \langle \sigma_j^z \rangle$, or use its own equation of motion, Eq. (D9).

In Fig. 10 we show the polarization dynamics of the first ensemble, obtained using the different approximation schemes (1)–(5). The Hartree, Wick, and Spin approximations are implemented without including the equations of motion for the zz correlations. As can be appreciated, these three approaches result in different dynamics that eventually converge to the same steady-state value as that obtained in the spin-temperature description. If we include the equations of motion for the zz correlations then the results are much better; see Fig. 11. Curiously enough, the best approximation for the first ensemble is the Spin approximation, while the best for the second is the Wick approximation. This can be understood as follows. In a rotated frame, we already established that the equation of
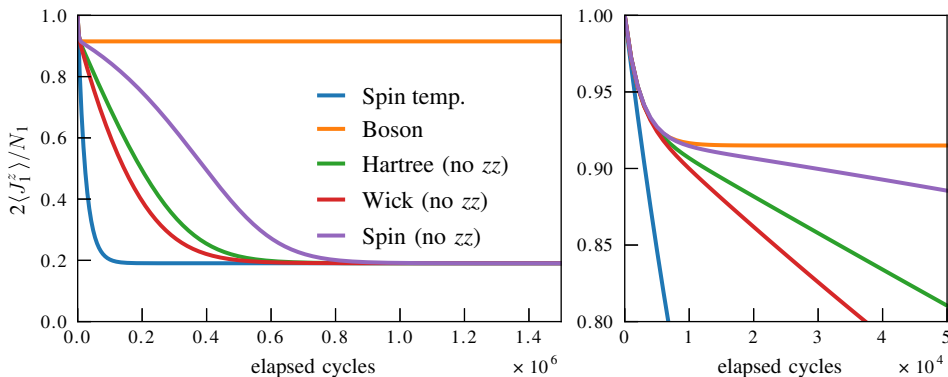

FIG. 10. Polarization dynamics for the first ensemble as given by the different approximation schemes. The plot on the right is just an enlargement of the short-term dynamics. The results correspond to a homogeneous system with parameters $N_1 = 50$, $\mu = 0.5/\sqrt{N_1}$, and $\nu = 0.8\mu$. The Hartree, Wick, and Spin approximations have been used without including the equations of motion for the zz correlations.
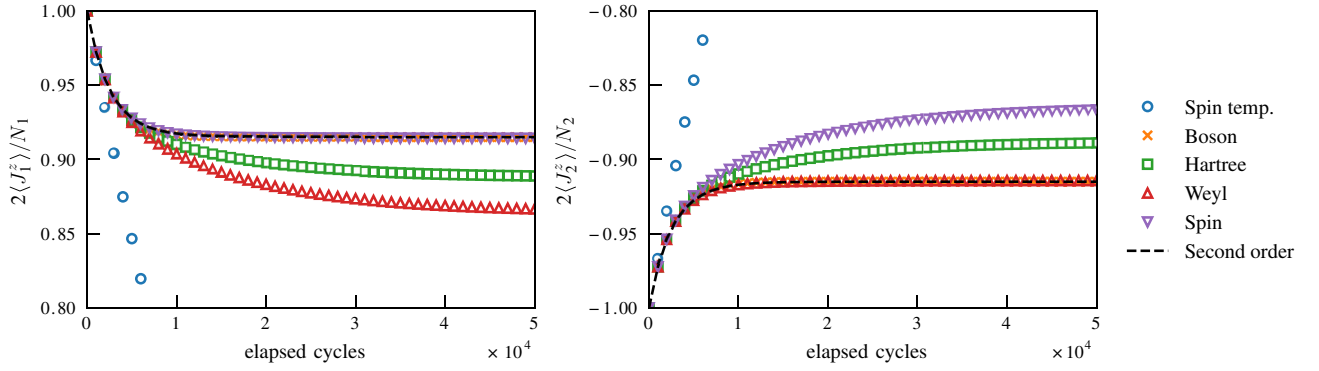
FIG. 11. Polarization in the first (left) and second (right) ensembles for an homogeneous system with $N_1 = N_2 = 50$, $\mu = 0.5/\sqrt{N_1}$, and $\nu = 0.8\mu$. The markers correspond to the different approximation schemes (1)–(5), while the dashed line corresponds to the result given by the second-order master equation, Eq. (3) in the main text.

motion of $\langle \tilde{\sigma}_{i2}^z \rangle$ is the same as that of $\langle \sigma_{i1}^z \rangle$. Applying the Spin approximation in this rotated frame amounts to

$$\langle \tilde{\sigma}_i^+ \tilde{\sigma}_j^z \tilde{\sigma}_k^- \rangle \approx \langle \tilde{\sigma}_j^z \rangle \langle \tilde{\sigma}_i^+ \tilde{\sigma}_k^- \rangle - 2\langle \tilde{\sigma}_i^+ \tilde{\sigma}_j^- \rangle \langle \tilde{\sigma}_j^+ \tilde{\sigma}_k^- \rangle$$

$$\text{for } i \neq j,\ j \neq k, \text{ and } i \neq k. \quad \text{(D13)}$$

Rotating back to the original frame we have

$$-\langle \sigma_i^- \sigma_j^z \sigma_k^+ \rangle \approx -\langle \sigma_j^z \rangle \langle \sigma_i^- \sigma_k^+ \rangle - 2\langle \sigma_i^- \sigma_j^+ \rangle \langle \sigma_j^- \sigma_k^+ \rangle$$

$$\text{for } i \neq j,\ j \neq k, \text{ and } i \neq k. \quad \text{(D14)}$$

Rearranging the operators, we then have

$$\langle \sigma_k^+ \sigma_j^z \sigma_i^- \rangle \approx \langle \sigma_j^z \rangle \langle \sigma_k^+ \sigma_i^- \rangle + 2\langle \sigma_j^+ \sigma_i^- \rangle \langle \sigma_k^+ \sigma_j^- \rangle$$

$$\text{for } i \neq j,\ j \neq k, \text{ and } i \neq k, \quad \text{(D15)}$$

which is nothing but the Wick approximation. We also note that the Boson approximation seems to be fine. However, as we show next, it is not so good for the variances.

2. Variance dynamics

Because of the symmetries of the protocol (we only send electrons polarized in the z direction), we expect $\text{var}(J_1^x + J_2^x) = \text{var}(J_1^y + J_2^y)$. The variance of the total nuclear spin along the x direction is

$$\text{var}(J_1^x + J_2^x)$$

$$= \frac{1}{4} \sum_{i,j,i',j'} \langle \sigma_{ij}^+ \sigma_{i'j'}^+ + \sigma_{ij}^+ \sigma_{i'j'}^- + \sigma_{ij}^- \sigma_{i'j'}^+ + \sigma_{ij}^- \sigma_{i'j'}^- \rangle$$

$$- \frac{1}{4}\left(\sum_{i,j} \langle \sigma_{ij}^+ + \sigma_{ij}^- \rangle \right)^2. \quad \text{(D16)}$$

Note that $\langle \sigma_{ij}^- \rangle = \langle \sigma_{ij}^+ \rangle^*$, $\langle \sigma_{ij}^- \sigma_{i'j'}^- \rangle = \langle \sigma_{i'j'}^+ \sigma_{ij}^+ \rangle^*$, and $\langle \sigma_{ij}^+ \sigma_{i'j'}^- \rangle = \langle \sigma_{i'j'}^+ \sigma_{ij}^- \rangle^*$ (z^* denotes the complex conjugate

of z). However, since the Liouvillian superoperator and the initial nuclei's reduced density matrix are both real, the covariance matrix is symmetric at all times, $\langle \sigma_{ij}^+ \sigma_{i'j'}^- \rangle = \langle \sigma_{i'j'}^+ \sigma_{ij}^- \rangle$. This property of the covariance matrix is also maintained by the equations of motion. Also, it can be shown that if $\langle \sigma_{ij}^+ \rangle$ and $\langle \sigma_{ij}^+ \sigma_{i'j'}^+ \rangle$ are zero initially, they remain equal to zero throughout time evolution. With this assumption, noting that $\{\sigma_{ij}^+, \sigma_{ij}^-\} = 1$, we have

$$\text{var}(J_1^x + J_2^x) = \frac{1}{2} \sum_{i,j \neq i',j'} \gamma_{ii'}^{jj'} + \frac{N_1 + N_2}{4}. \quad \text{(D17)}$$

We have already worked out the equations of motion of γ_{ij}^{11} and γ_{ij}^{22} in the previous section, and found the best approximations to compute them, namely,

$$\langle \sigma_{i1}^+ \sigma_{j1}^z \sigma_{k1}^- \rangle \approx (2\gamma_{jj}^{11} - 1)\gamma_{ik}^{11} - 2\gamma_{ij}^{11}\gamma_{jk}^{11},$$

$$\langle \sigma_{i2}^+ \sigma_{j2}^z \sigma_{k2}^- \rangle \approx (2\gamma_{jj}^{22} - 2)\gamma_{ik}^{22} + 2\gamma_{ij}^{22}\gamma_{jk}^{22} \quad \text{(D18)}$$

for $i \neq j$, $j \neq k$, and $i \neq k$. However, the remaining covariance matrix elements depend on higher-order correlations of spins belonging to different ensembles, as can be seen in their equations of motion

$$\Delta\gamma_{ij}^{12} = -\kappa \sum_{k \neq i} g_{k1}g_{i1} \langle \sigma_{k1}^+ \sigma_{i1}^z \sigma_{j2}^- \rangle$$

$$- \sum_{k \neq j} g_{k2}g_{j2} \langle \sigma_{i1}^+ \sigma_{j2}^z \sigma_{k2}^- \rangle - \eta(g_{i1}^2 + g_{j2}^2)\gamma_{ij}^{12}$$

$$+ \frac{\mu\nu}{4} g_{i1}g_{j2}\lambda_{ij}^{12}, \quad \text{(D19)}$$

$$\Delta\lambda_{ij}^{12} = 2\kappa \sum_{k\neq i} g_{k1}g_{i1}(\langle\sigma_{i1}^+\sigma_{j2}^z\sigma_{k1}^-\rangle + \langle\sigma_{k1}^+\sigma_{j2}^z\sigma_{i1}^-\rangle)$$

$$- 2\kappa \sum_{k\neq j} g_{k2}g_{j2}(\langle\sigma_{j2}^+\sigma_{i1}^z\sigma_{k2}^-\rangle + \langle\sigma_{k2}^+\sigma_{i1}^z\sigma_{j2}^-\rangle)$$

$$- 2\eta(g_{i1}^2 + g_{j2}^2)\lambda_{ij}^{12} + \mu\nu g_{i1}g_{j2}(\gamma_{ji}^{21} + \gamma_{ij}^{12})$$

$$- 2\kappa[g_{j2}^2(2\gamma_{ii}^{11}-1) - g_{i1}^2(2\gamma_{jj}^{22}-1)]. \quad \text{(D20)}$$

Below, we discuss several approaches to close the equations of motion and compute γ_{ij}^{12}.

(1) *Spin temperature.* In this approach we neglect all correlations between different nuclei, so $\gamma_{ii'}^{jj'} \approx 0$, and the variance is simply given by $\mathrm{var}(J_1^x + J_2^x) \approx (N_1 + N_2)/4$.

(2) *Boson.* Approximating $[\sigma_{i1}^+, \sigma_{j1}^-] \approx \delta_{ij}$ and $[\sigma_{i1}^+, \sigma_{j2}^-] \approx -\delta_{ij}$, we directly obtain from the second-order master equation the following closed system of equations:

$$\Delta\gamma_{ij}^{12} = -\kappa\left(\sum_k g_{k1}g_{i1}\gamma_{kj}^{12} + \sum_k g_{k2}g_{j2}\gamma_{ik}^{12}\right) - \frac{\mu\nu}{4}g_{i1}g_{j2}.$$

$$\text{(D21)}$$

(3) *Hartree.* As can be appreciated, in Fig. 11, the Hartree approximation lies in between the Spin and the Wick approximations. Thus, we may approximate higher-order correlations that involve spins in different ensembles using the Hartree approximation.

(4) *Half-Hartree.* Approximate $\langle\sigma_{ij}^+\sigma_{i'j'}^z\sigma_{kl}^-\rangle$ using the Hartree approximation if $j \neq l$, and the Spin (Wick) approximation if $j = l = 1$ ($j = l = 2$).

(5) *Majority.* Approximate higher-order correlations that involve spins in different ensembles using the Spin (Wick) approximation if the majority of operators belong to the first (second) ensemble.

(6) *Z rules.* Approximate $\langle\sigma_{ij}^+\sigma_{i'j'}^z\sigma_{kl}^-\rangle$ using the Spin (Wick) approximation if $j' = 1$ ($j' = 2$).

In Fig. 12 we show the resulting dynamics of the transverse spin variance for an homogeneous system with ensemble sizes $N_1 = N_2 = 5$ (left) and $N_1 = N_2 = 50$ (right). All approximations seem to work better for the larger system. Among all of them, the closest to the actual dynamics is the Z-rules approximation.

As a final check, we compare the dynamics given by the Z-rules approximation with the actual dynamics given by the second-order master equation for a small inhomogeneous system; see Fig. 13. While the polarizations seem to be very well approximated by the equations of motion, the variances are a bit underestimated. However, as we show in Fig. 12, calculations for homogeneous systems of different sizes suggest that this difference could be less significant the larger the size of the ensembles. Remarkably, all different initial states considered converge to the same steady state.

APPENDIX E: SHELL MODEL

In a shell model, we partition each nuclear ensemble into groups of nuclei that we call "shells." The nuclei in each shell have similar coupling constants, and are specified by the sets $\mathcal{S}_\alpha^j = \{i \in \mathrm{QD}j : g_{ij} \in [g_\alpha, g_{\alpha+1}]\}$ (we use Greek indices to label different shells). For all $i \in \mathcal{S}_\alpha^j$, we approximate $g_{ij} \simeq g_{\alpha j}$, where $g_{\alpha j}$ is the average coupling strength of the nuclei in shell $\mathcal{S}_\alpha^j$. As explained in the main text, for some initial states, the correlations are the same for all the nuclei inside a given shell: $\gamma_{ii}^{jj} = x_\alpha^j$ for all $i \in \mathcal{S}_\alpha^j$; $\gamma_{ii'}^{jj'} = y_{\alpha\beta}^{jj'}$ for all $i \in \mathcal{S}_\alpha^j, i' \in \mathcal{S}_\beta^{j'}, (i,j) \neq (i',j')$; and $\lambda_{ii'}^{jj'} = z_{\alpha\beta}^{jj'}$ for all $i \in \mathcal{S}_\alpha^j, i' \in \mathcal{S}_\beta^{j'}, (i,j) \neq (i',j')$. From
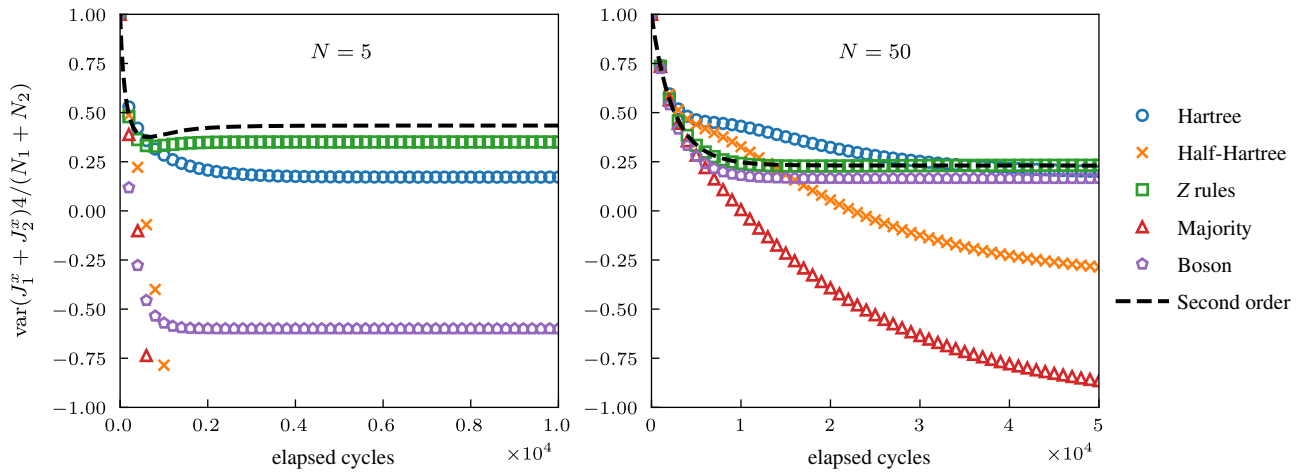

FIG. 12. Variance of the total spin along a transverse direction for homogeneous systems with $N_1 = N_2 = N$, $\mu = 0.5/\sqrt{N}$, and $\nu = 0.8/\mu$. The markers correspond to approximation schemes (2)–(6), while the dashed line corresponds to the result given by the second-order master equation.
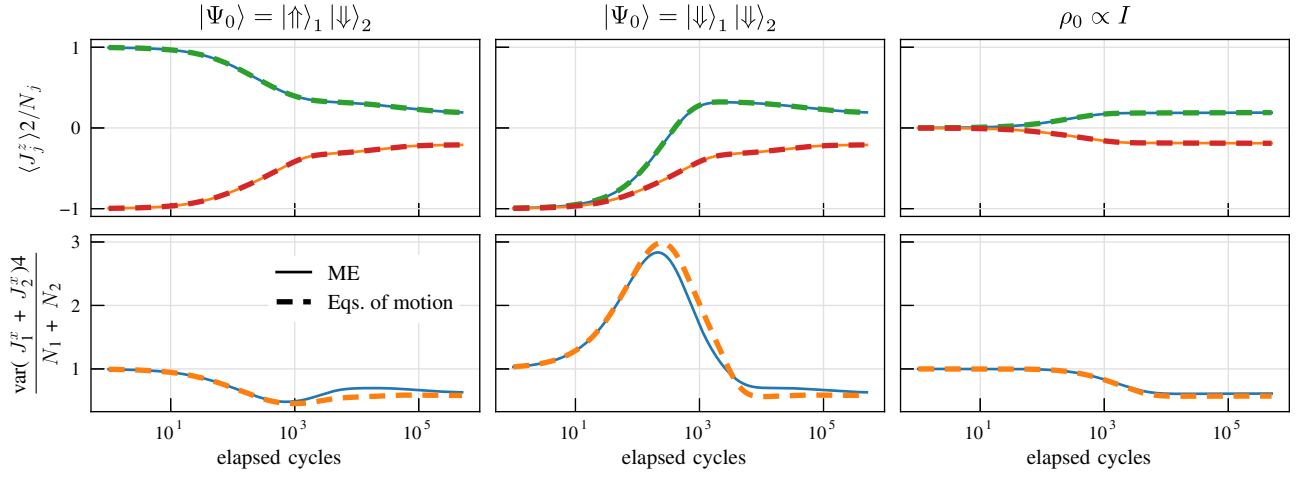
FIG. 13.　Evolution of the polarizations of each ensemble and variance of the total spin in the transverse plane for an inhomogeneous system with $N_1 = N_2 = 5$. Each column corresponds to a different initial state ($\rho_0 = |\Psi_0\rangle \langle \Psi_0|$). Continuous lines show the results obtained using the second-order master equation [Eq. (3) in the main text], while dashed lines show the results given by the equations of motion [Eqs. (12) and (13) in the main text]. The coupling constants are all different and they have a relative standard deviation of 32% for the first ensemble, and 51% for the second; they are the same for all different initial states considered. The remaining parameters have values $\mu = 0.5/\sqrt{N_1}$ and $\nu = 0.8\mu$.

Eqs. (D7)–(D9) (and the equivalent equations of motion for QD2), using the Z-rules approximation, we obtain the following set of equations:

$$\Delta x_\alpha^j = -(-1)^j \kappa g_{\alpha j}(2S_\alpha^j + g_{\alpha j}) - \eta g_{\alpha j}^2 (2x_\alpha^j - 1), \quad \text{(E1)}$$

$$\begin{aligned}
\Delta y_{\alpha\beta}^{jj} = (-1)^j \kappa [& g_{\beta j}(2x_\beta^j - 1)S_{\alpha\beta}^j + g_{\alpha j}(2x_\alpha^j - 1)S_{\beta\alpha}^j \\
& + g_{\alpha j} g_{\beta j}(x_\alpha^j + x_\beta^j - 1)] \\
& + 2\kappa(g_{\alpha j} S_{\alpha\beta}^j + g_{\beta j} S_{\beta\alpha}^j)y_{\alpha\beta}^{jj} - \eta(g_{\alpha j}^2 + g_{\beta j}^2)y_{\alpha\beta}^{jj} \\
& + \eta g_{\alpha j} g_{\beta j} z_{\alpha\beta}^j, \quad \text{(E2)}
\end{aligned}$$

$$\begin{aligned}
\Delta z_{\alpha\beta}^{jj} = -(-1)^j 2\kappa [& g_{\alpha j}(2x_\beta^j - 1)(2S_{\alpha\beta}^j + g_{\alpha j}) \\
& + g_{\beta j}(2x_\alpha^j - 1)(2S_{\beta\alpha}^j + g_{\beta j})] \\
& - 8\kappa(g_{\beta j} S_{\alpha\beta}^j + g_{\alpha j} S_{\beta\alpha}^j)y_{\alpha\beta}^{jj} + 8\eta g_{\alpha j} g_{\beta j} y_{\alpha\beta}^{jj} \\
& - 2\eta(g_{\alpha j}^2 + g_{\beta j}^2)z_{\alpha\beta}^{jj}. \quad \text{(E3)}
\end{aligned}$$

Here, we have defined $S_\alpha^j = \sum_\gamma g_{\gamma j} N_\gamma^j y_{\alpha\gamma}^{jj} - g_{\alpha j} y_{\alpha\alpha}^{jj}$ and $S_{\alpha\beta}^j = S_\alpha^j - g_{\beta j} y_{\alpha\beta}^{jj}$; N_α^j denotes the number of nuclei in shell $\mathcal{S}_\alpha^j$. Note that it only makes sense to consider $y_{\alpha\alpha}^{jj}$ and $z_{\alpha\alpha}^{jj}$ if $N_\alpha^j > 1$; otherwise, we should set $y_{\alpha\alpha}^{jj} = z_{\alpha\alpha}^{jj} = 0$. For variables involving shells in different QDs, from Eqs. (D19) and (D20), using the Z-rules approximation,

we obtain the equations

$$\begin{aligned}
\Delta y_{\alpha\beta}^{12} = & -\kappa g_{\alpha 1}[(2x_\alpha^1 - 1)A_{\alpha\beta} - 2y_{\alpha\beta}^{12} S_\alpha^1] \\
& + \kappa g_{\beta 2}[(2x_\beta^2 - 1)B_{\alpha\beta} + 2y_{\alpha\beta}^{12} S_\beta^2] \\
& - \eta(g_{\alpha 1}^2 + g_{\beta 2}^2)y_{\alpha\beta}^{12} + \frac{\mu\nu}{4} g_{\alpha 1} g_{\beta 2} z_{\alpha\beta}^{12}, \quad \text{(E4)}
\end{aligned}$$

$$\begin{aligned}
\Delta z_{\alpha\beta}^{12} = & 4\kappa g_{\alpha 1}[(2x_\beta^2 - 1)S_\alpha^1 + 2y_{\alpha\beta}^{12} A_{\alpha\beta}] \\
& - 4\kappa g_{\beta 2}[(2x_\alpha^1 - 1)S_\beta^2 - 2y_{\alpha\beta}^{12} B_{\alpha\beta}] \\
& - 2\eta(g_{\alpha 1}^2 + g_{\beta 2}^2)z_{\alpha\beta}^{12} + 2\mu\nu g_{\alpha 1} g_{\beta 2} y_{\alpha\beta}^{12} \\
& - 2\kappa[g_{\beta 2}^2(2x_\alpha^1 - 1) - g_{\alpha 1}^2(2x_\beta^2 - 1)], \quad \text{(E5)}
\end{aligned}$$

where we have defined $A_{\alpha\beta} = \sum_\gamma g_{\gamma 1} N_\gamma^1 y_{\gamma\beta}^{12} - g_{\alpha 1} y_{\alpha\beta}^{12}$ and $B_{\alpha\beta} = \sum_\gamma g_{\gamma 2} N_\gamma^2 y_{\alpha\gamma}^{12} - g_{\beta 2} y_{\alpha\beta}^{12}$.

The steady state is a solution of $\Delta x_\alpha^j = 0$, $\Delta y_{\alpha\beta}^{jj'} = 0$, and $\Delta z_{\alpha\beta}^{jj'} = 0$. Looking at this set of equations, we realize that $\Delta z_{\alpha\alpha}^{jj} = -4\Delta y_{\alpha\alpha}^{jj}$, so the system is underdetermined. Nonetheless, at any given step n,

$$z_{\alpha\alpha}^{jj}(n+1) = z_{\alpha\alpha}^{jj}(n) + \Delta z_{\alpha\alpha}^{jj}(n) = z_{\alpha\alpha}^{jj}(n) - 4\Delta y_{\alpha\alpha}^{jj}(n), \quad \text{(E6)}$$

so the steady-state solution satisfies $z_{\alpha\alpha}^{jj} = z_{\alpha\alpha}^{jj}(0) - 4[y_{\alpha\alpha}^{jj} - y_{\alpha\alpha}^{jj}(0)]$, where $y_{\alpha\alpha}^{jj}(0)$ and $z_{\alpha\alpha}^{jj}(0)$ are the initial values of the corresponding variables. In this manner, the steady state depends on the initial state.

For a fully polarized initial state $\rho_0 = |\Psi_{FP}\rangle\langle\Psi_{FP}|$, $|\Psi_{FP}\rangle \equiv |\Uparrow\rangle_1|\Downarrow\rangle_2$, the initial covariance matrix elements and zz correlations are $\gamma_{ii}^{11} = 1$, $\gamma_{ii}^{22} = 0$, $\gamma_{ii'}^{jj'} = 0$, for $(i,j) \neq (i',j')$; $\lambda_{ii'}^{jj} = 1$; and $\lambda_{ij}^{12} = -1$. For this particular initial state, we find numerically that the steady state is such that $y_{\alpha\beta}^{jj} = 0$ for $\alpha \neq \beta$. Substituting $y_{\alpha\beta}^{jj} = 0$ back in Eqs. (E1)–(E3), we obtain

$$2x_\alpha^j - 1 = -(-1)^j \frac{\kappa}{\eta}[2(N_\alpha^j - 1)y_{\alpha\alpha}^{jj} + 1], \tag{E7}$$

$$4\kappa(N_\alpha^j - 2)[\kappa(N_\alpha^j - 1) - \eta](y_{\alpha\alpha}^{jj})^2$$
$$+ [2\kappa^2(2N_\alpha^j - 3) + 6\eta^2]y_{\alpha\alpha}^{jj} + \kappa^2 - \eta^2 = 0. \tag{E8}$$

Thus, the steady-state polarization of each shell is independent of the others, and it can be found by solving a single quadratic equation. It depends on the values of μ and ν and the number of nuclei in shell N_α^j, but not on its coupling constant $g_{\alpha j}$. Having found the steady-state values of x_α^j and $y_{\alpha\beta}^{jj}$, we can substitute them back into Eqs. (E4) and (E5) and use a numerical algorithm to find the steady-state values of $y_{\alpha\beta}^{12}$ (we used the version of the Levenberg-Marquardt algorithm provided by the PYTHON function `scipy.optim.root` with the option `method='lm'`). As an example, in Fig. 14 we show the dynamics of a system where we model the electronic wave function with a Gaussian. The two ensembles consist of

$N_1 = 21$ and $N_2 = 25$ nuclei arranged in a square lattice. In one of the cases considered, the electronic wave function in each QD is centered with respect to the nuclear lattice, so that many nuclei have the same coupling constant. Therefore, this case can be described exactly with few shells containing several nuclei each. In the other case, the electronic wave function in QD1 has the same shape, but it has been displaced a little bit away from the center of the nuclear lattice, resulting in many different values of the coupling constants; we model the dynamics directly using the equations of motion, Eqs. (12) and (13), without making any shell approximation. The former case features a higher value of the nuclear polarizations, a lower value of the transverse spin variances, and a value of $\Delta_{EPR} < 1$ in the steady state, which is reached within the computed time span. The second case, on the other hand, does not present an entangled steady state but metastable entanglement for many cycles. As can be seen, the dynamics of both cases are almost identical up to times of the order of 10^5 cycles.

In Fig. 15, we compare the two entanglement witnesses Δ and Δ_{EPR} for the system analyzed in Fig. 4 in the main text. We also show the evolution of some of the quantities needed to compute them, which present interesting differences. The polarization $\langle J_1^z \rangle$ reaches a fixed steady-state value, the same for all the different cases considered. This is consistent with the fact that the steady-state polarization of each shell is independent of the couplings. By contrast, in $\langle A_1^{(z,2)} \rangle$ the shell polarizations are weighted by
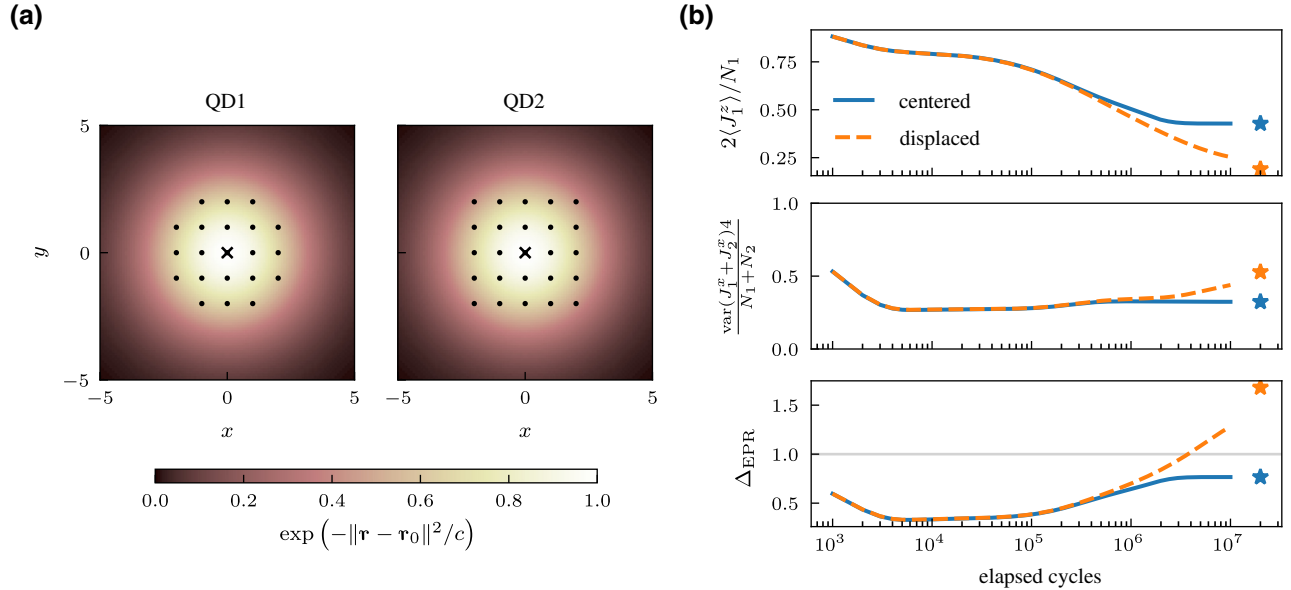

FIG. 14. (a) Schematics of the system under consideration. Each ensemble has a total of $N_1 = 21$ and $N_2 = 25$ nuclei, arranged in a lattice as shown by the black dots, with coupling constants proportional to a Gaussian function (colormap). The center of the Gaussian is indicated by a black cross. The case shown corresponds to the "centered" system. (b) Comparison between the dynamics of such a system in the case in which the Gaussian function is centered with respect to the lattice of nuclei, $\mathbf{r}_{0,j} = (0,0)$ ($j = 1, 2$), and in the case it is shifted a little bit away from the center in QD1, $\mathbf{r}_{0,1} = (0.2, 0.1)$, $\mathbf{r}_{0,2} = (0,0)$. In both cases the spread of the function is the same, $c = 10$. The stars on the right-hand side of the plot mark the steady-state values of the corresponding quantities. The rest of the parameters are in both cases $\mu = 0.5/\sqrt{N_1}$ and $\nu = 0.8\mu$, and the initial state is $\rho_0 = |\Psi_{FP}\rangle\langle\Psi_{FP}|$.
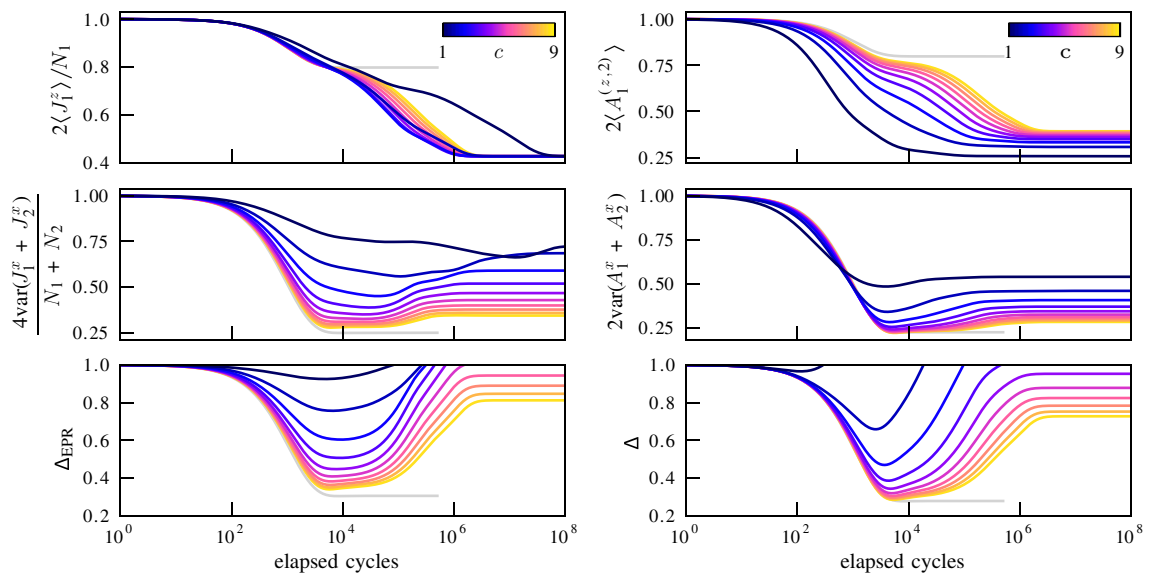
FIG. 15.   Comparison between the two entanglement witnesses Δ and Δ_{EPR} for the same system as in Fig. 4 of the main text.

their respective couplings squared, such that its steady-state value is different in every case considered. Also, note how the curves for the more inhomogeneous cases seem to reach the steady-state value much faster than the homologous curves for $\langle J_1^z \rangle$. This suggests that the more weakly coupled spins are the ones that take longer to stabilize. As we can see, Δ detects more cases than Δ_{EPR} to be entangled in the steady state.

[1] J. Schliemann, A. Khaetskii, and D. Loss, Electron spin dynamics in quantum dots and related nanostructures due to hyperfine interaction with nuclei, J. Phys.: Condens. Matter **15**, R1809 (2003).

[2] J. Iñarrea, G. Platero, and A. H. MacDonald, Electronic transport through a double quantum dot in the spin-blockade regime: Theoretical models, Phys. Rev. B **76**, 085329 (2007).

[3] E. A. Chekhovich, M. N. Makhonin, A. I. Tartakovskii, A. Yacoby, H. Bluhm, K. C. Nowack, and L. M. K. Vandersypen, Nuclear spin effects in semiconductor quantum dots, Nat. Mater. **12**, 494 (2013).

[4] H. Bluhm, S. Foletti, I. Neder, M. Rudner, D. Mahalu, V. Umansky, and A. Yacoby, Dephasing time of GaAs electron-spin qubits coupled to a nuclear bath exceeding 200 μs, Nat. Phys. **7**, 109 (2011).

[5] F. K. Malinowski, F. Martins, P. D. Nissen, E. Barnes, M. S. Rudner, S. Fallahi, G. C. Gardner, M. J. Manfra, C. M. Marcus, and F. Kuemmeth, Notch filtering the nuclear environment of a spin qubit, Nat. Nanotechnol. **12**, 16 (2017).

[6] L. R. Schreiber and H. Bluhm, Quantum computation: Silicon comes back, Nat. Nanotechnol. **9**, 966 (2014).

[7] A. M. Waeber, M. Hopkinson, I. Farrer, D. A. Ritchie, J. Nilsson, R. M. Stevenson, A. J. Bennett, A. J. Shields,

G. Burkard, A. I. Tartakovskii, M. S. Skolnick, and E. A. Chekhovich, Few-second-long correlation times in a quantum dot nuclear spin bath probed by frequency-comb nuclear magnetic resonance spectroscopy, Nat. Phys. **12**, 688 (2016).

[8] D. A. Gangloff, G. Éthier-Majcher, C. Lang, E. V. Denning, J. H. Bodey, D. M. Jackson, E. Clarke, M. Hugues, C. Le Gall, and M. Atatüre, Quantum interface of an electron and a nuclear ensemble, Science **364**, 62 (2019).

[9] P. Simon and D. Loss, Nuclear Spin Ferromagnetic Phase Transition in an Interacting 2D Electron Gas, Phys. Rev. Lett. **98**, 156401 (2007).

[10] J. Danon, I. T. Vink, F. H. L. Koppens, K. C. Nowack, L. M. K. Vandersypen, and Y. V. Nazarov, Multiple Nuclear Polarization States in a Double Quantum Dot, Phys. Rev. Lett. **103**, 046601 (2009).

[11] M. S. Rudner and L. S. Levitov, Phase transitions in dissipative quantum transport and mesoscopic nuclear spin pumping, Phys. Rev. B **82**, 155418 (2010).

[12] O. Krebs, P. Maletinsky, T. Amand, B. Urbaszek, A. Lemaître, P. Voisin, X. Marie, and A. Imamoglu, Anomalous Hanle Effect Due to Optically Created Transverse Overhauser Field in Single InAs/GaAs Quantum Dots, Phys. Rev. Lett. **104**, 056603 (2010).

[13] M. S. Rudner, L. M. K. Vandersypen, V. Vuletić, and L. S. Levitov, Generating Entanglement and Squeezed States of Nuclear Spins in Quantum Dots, Phys. Rev. Lett. **107**, 206806 (2011).

[14] E. M. Kessler, G. Giedke, A. Imamoğlu, S. F. Yelin, M. D. Lukin, and J. I. Cirac, Dissipative phase transition in central spin systems, Phys. Rev. A **86**, 012116 (2012).

[15] M. S. Rudner and L. S. Levitov, Self-Sustaining Dynamical Nuclear Polarization Oscillations in Quantum Dots, Phys. Rev. Lett. **110**, 086601 (2013).

[16] A. M. Lunde, C. López-Monís, I. A. Vasiliadou, L. L. Bonilla, and G. Platero, Temperature-dependent dynamical

nuclear polarization bistabilities in double quantum dots in the spin-blockade regime, Phys. Rev. B **88,** 035317 (2013).

[17] Y. Kondo, S. Amaha, K. Ono, K. Kono, and S. Tarucha, Critical Behavior of Alternately Pumped Nuclear Spins in Quantum Dots, Phys. Rev. Lett. **115,** 186803 (2015).

[18] A. V. Shumilin and D. S. Smirnov, Nuclear Spin Dynamics, Noise, Squeezing, and Entanglement in Box Model, Phys. Rev. Lett. **126,** 216804 (2021).

[19] V. V. Dobrovitski, J. M. Taylor, and M. D. Lukin, Long-lived memory for electronic spin in a quantum dot: Numerical analysis, Phys. Rev. B **73,** 245318 (2006).

[20] W. M. Witzel and S. Das Sarma, Nuclear spins as quantum memory in semiconductor nanostructures, Phys. Rev. B **76,** 045218 (2007).

[21] Z. Kurucz, M. W. Sørensen, J. M. Taylor, M. D. Lukin, and M. Fleischhauer, Qubit Protection in Nuclear-Spin Quantum Dot Memories, Phys. Rev. Lett. **103,** 010502 (2009).

[22] E. V. Denning, D. A. Gangloff, M. Atatüre, J. Mørk, and C. Le Gall, Collective Quantum Memory Activated by a Driven Central Spin, Phys. Rev. Lett. **123,** 140502 (2019).

[23] J. M. Taylor, C. M. Marcus, and M. D. Lukin, Long-Lived Memory for Mesoscopic Quantum Bits, Phys. Rev. Lett. **90,** 206803 (2003).

[24] B. Hensen, W. Wei Huang, C.-H. Yang, K. Wai Chan, J. Yoneda, T. Tanttu, F. E. Hudson, A. Laucht, K. M. Itoh, T. D. Ladd, A. Morello, and A. S. Dzurak, A silicon quantum-dot-coupled nuclear spin qubit, Nat. Nanotechnol. **15,** 13 (2020).

[25] M. J. A. Schuetz, E. M. Kessler, L. M. K. Vandersypen, J. I. Cirac, and G. Giedke, Steady-State Entanglement in the Nuclear Spin Dynamics of a Double Quantum Dot, Phys. Rev. Lett. **111,** 246802 (2013).

[26] M. J. A. Schuetz, E. M. Kessler, L. M. K. Vandersypen, J. I. Cirac, and G. Giedke, Nuclear spin dynamics in double quantum dots: Multistability, dynamical polarization, criticality, and entanglement, Phys. Rev. B **89,** 195310 (2014).

[27] M. Benito, M. J. A. Schuetz, J. I. Cirac, G. Platero, and G. Giedke, Dissipative long-range entanglement generation between electronic spins, Phys. Rev. B **94,** 115404 (2016).

[28] G. Yang, C.-H. Hsu, P. Stano, J. Klinovaja, and D. Loss, Long-distance entanglement of spin qubits via quantum Hall edge states, Phys. Rev. B **93,** 075301 (2016).

[29] T. A. Baart, M. Shafiei, T. Fujita, C. Reichl, W. Wegscheider, and L. M. K. Vandersypen, Single-spin CCD, Nat. Nanotechnol. **11,** 330 (2016).

[30] Y. Ban, X. Chen, S. Kohler, and G. Platero, Spin entangled state transfer in quantum dot arrays: Coherent adiabatic and speed-up protocols, Adv. Quantum Technol. **2,** 1900048 (2019).

[31] A. R. Mills, D. M. Zajac, M. J. Gullans, F. J. Schupp, T. M. Hazard, and J. R. Petta, Shuttling a single charge across a one-dimensional array of silicon quantum dots, Nat. Commun. **10,** 1063 (2019).

[32] J. Yoneda, W. Huang, M. Feng, C. H. Yang, K. W. Chan, T. Tanttu, W. Gilbert, R. C. C. Leon, F. E. Hudson, K. M. Itoh, A. Morello, S. D. Bartlett, A. Laucht, A. Saraiva, and A. S. Dzurak, Coherent spin qubit transport in silicon, Nat. Commun. **12,** 4114 (2021).

[33] C. Bäuerle, D. C. Glattli, T. Meunier, F. Portier, P. Roche, P. Roulleau, S. Takada, and X. Waintal, Coherent control of single electrons: A review of current progress, Rep. Prog. Phys. **81,** 056503 (2018).

[34] S. Takada, H. Edlbauer, H. V. Lepage, J. Wang, P.-A. Mortemousque, G. Georgiou, C. H. W. Barnes, C. J. B. Ford, M. Yuan, P. V. Santos, X. Waintal, A. Ludwig, A. D. Wieck, M. Urdampilleta, T. Meunier, and C. Bäuerle, Sound-driven single-electron transfer in a circuit of coupled quantum rails, Nat. Commun. **10,** 4557 (2019).

[35] B. Jadot, P.-A. Mortemousque, E. Chanrion, V. Thiney, A. Ludwig, A. D. Wieck, M. Urdampilleta, C. Bäuerle, and T. Meunier, Distant spin entanglement via fast and coherent electron shuttling, Nat. Nanotech. **16,** 570 (2021).

[36] D. M. Jackson, D. A. Gangloff, J. H. Bodey, L. Zaporski, C. Bachorz, E. Clarke, M. Hugues, C. L. Gall, and M. Atatüre, Quantum sensing of a coherent single spin excitation in a nuclear ensemble, Nat. Phys. **17,** 585 (2021).

[37] S. Asaad, V. Mourik, B. Joecker, M. A. I. Johnson, A. D. Baczewski, H. R. Firgau, M. T. Mądzik, V. Schmitt, J. J. Pla, F. E. Hudson, K. M. Itoh, J. C. McCallum, A. S. Dzurak, A. Laucht, and A. Morello, Coherent electrical control of a single high-spin nucleus in silicon, Nature **579,** 205 (2020).

[38] Usually, the contact hyperfine interaction in quantum dots is written as $H = A_H \sum_i \alpha_i \mathbf{I}_i \cdot \mathbf{S}$, where α_i gives the relative coupling to the ith nucleus, $\sum_i \alpha_i = 1$. Instead, we use an equivalent parametrization of the hyperfine interaction in terms of collective spin operators $A_j^{\pm}$, which approximately satisfy bosonic commutation relations $\langle [A_j^-, A_j^+] \rangle \approx (-1)^j$ for highly polarized nuclear states. This simplifies the subsequent analysis of the protocol based on the Holstein-Primakoff approximation.

[39] P. Philippopoulos, S. Chesi, and W. A. Coish, First-principles hyperfine tensors for electrons and holes in GaAs and silicon, Phys. Rev. B **101,** 115302 (2020).

[40] W. A. Coish and J. Baugh, Nuclear spins in nanostructures, Phys. Status Solidi (B) **246,** 2203 (2009).

[41] L. V. C. Assali, H. M. Petrilli, R. B. Capaz, B. Koiller, X. Hu, and S. Das Sarma, Hyperfine interactions in silicon quantum dots, Phys. Rev. B **83,** 165301 (2011).

[42] C. A. Muschik, E. S. Polzik, and J. I. Cirac, Dissipatively driven entanglement of two macroscopic atomic ensembles, Phys. Rev. A **83,** 052312 (2011).

[43] H. Krauter, C. A. Muschik, K. Jensen, W. Wasilewski, J. M. Petersen, J. I. Cirac, and E. S. Polzik, Entanglement Generated by Dissipation and Steady State Entanglement of Two Macroscopic Objects, Phys. Rev. Lett. **107,** 080503 (2011).

[44] M. G. Raymer, A. C. Funk, B. C. Sanders, and H. de Guise, Separability criterion for separate quantum systems, Phys. Rev. A **67,** 052104 (2003).

[45] F. Xue, D. P. Weber, P. Peddibhotla, and M. Poggio, Measurement of statistical nuclear spin polarization in a nanoscale GaAs sample, Phys. Rev. B **84,** 205328 (2011).

[46] O. Gittsovich, O. Gühne, P. Hyllus, and J. Eisert, Unifying several separability conditions using the covariance matrix criterion, Phys. Rev. A **78,** 052319 (2008).

[47] V. Tripathi, C. Radhakrishnan, and T. Byrnes, Covariance matrix entanglement criterion for an arbitrary set of operators, New J. Phys. **22**, 073055 (2020).

[48] G. S. Thekkadath, L. Jiang, and J. H. Thywissen, Spin correlations and entanglement in partially magnetised ensembles of fermions, J. Phys. B: Atom. Mol. Opt. Phys. **49**, 214002 (2016).

[49] J. Ma, X. Wang, C. Sun, and F. Nori, Quantum spin squeezing, Phys. Rep. **509**, 89 (2011).

[50] F. T. Arecchi, E. Courtens, R. Gilmore, and H. Thomas, Atomic coherent states in quantum optics, Phys. Rev. A **6**, 2211 (1972).

[51] T. Holstein and H. Primakoff, Field dependence of the intrinsic domain magnetization of a ferromagnet, Phys. Rev. **58**, 1098 (1940).

[52] H. Christ, J. I. Cirac, and G. Giedke, Quantum description of nuclear spin cooling in a quantum dot, Phys. Rev. B **75**, 155324 (2007).

[53] M. Gullans, J. J. Krich, J. M. Taylor, B. I. Halperin, and M. D. Lukin, Preparation of non-equilibrium nuclear spin states in double quantum dots, Phys. Rev. B **88**, 035309 (2013).

[54] S. E. Economou and E. Barnes, Theory of dynamic nuclear polarization and feedback in quantum dots, Phys. Rev. B **89**, 165301 (2014).

[55] A. Karabanov, D. Wiśniewski, I. Lesanovsky, and W. Köckenberger, Dynamic Nuclear Polarization as Kinetically Constrained Diffusion, Phys. Rev. Lett. **115**, 020404 (2015).

[56] J. M. Nichol, S. P. Harvey, M. D. Shulman, A. Pal, V. Umansky, E. I. Rashba, B. I. Halperin, and A. Yacoby, Quenching of dynamic nuclear polarization by spin-orbit coupling in GaAs quantum dots, Nat. Commun. **6**, 7682 (2015).

[57] G. Petersen, E. A. Hoffmann, D. Schuh, W. Wegscheider, G. Giedke, and S. Ludwig, Large Nuclear Spin Polarization in Gate-Defined Quantum Dots Using a Single-Domain Nanomagnet, Phys. Rev. Lett. **110**, 177602 (2013).

[58] E. A. Chekhovich, A. Ulhaq, E. Zallo, F. Ding, O. G. Schmidt, and M. S. Skolnick, Measurement of the spin temperature of optically cooled nuclei and GaAs hyperfine constants in GaAs/AlGaAs quantum dots, Nat. Mater. **16**, 982 (2017).

[59] J. Hildmann, E. Kavousanaki, G. Burkard, and H. Ribeiro, Quantum limit for nuclear spin polarization in semiconductor quantum dots, Phys. Rev. B **89**, 205302 (2014).

[60] A. Peres, Separability Criterion for Density Matrices, Phys. Rev. Lett. **77**, 1413 (1996).

[61] M. Horodecki, P. Horodecki, and R. Horodecki, Separability of mixed states: Necessary and sufficient conditions, Phys. Lett. A **223**, 1 (1996).

[62] O. Gühne and G. Tóth, Entanglement detection, Phys. Rep. **474**, 1 (2009).

[63] R. Hanson, L. M. K. Vandersypen, L. H. W. van Beveren, J. M. Elzerman, I. T. Vink, and L. P. Kouwenhoven, Semiconductor few-electron quantum dot operated as a bipolar spin filter, Phys. Rev. B **70**, 241304(R) (2004).

[64] E. Cota, R. Aguado, and G. Platero, ac-Driven Double Quantum Dots as Spin Pumps and Spin Filters, Phys. Rev. Lett. **94**, 107202 (2005).

[65] M. Busl and G. Platero, Spin-polarized currents in double and triple quantum dots driven by ac magnetic fields, Phys. Rev. B **82**, 205304 (2010).

[66] B. Jadot, P.-A. Mortemousque, E. Chanrion, V. Thiney, A. Ludwig, A. D. Wieck, M. Urdampilleta, C. Bäuerle, and T. Meunier, Distant spin entanglement via fast and coherent electron shuttling, Nat. Nanotechnol. **16**, 570 (2021).

[67] S. Büyükköse, B. Vratzov, J. van der Veen, P. V. Santos, and W. G. van der Wiel, Ultrahigh-frequency surface acoustic wave generation for acoustic charge transport in silicon, Appl. Phys. Lett. **102**, 013112 (2013).

[68] A. M. Tyryshkin, S. Tojo, J. J. L. Morton, H. Riemann, N. V. Abrosimov, P. Becker, H.-J. Pohl, T. Schenkel, M. L. W. Thewalt, K. M. Itoh, and S. A. Lyon, Electron spin coherence exceeding seconds in high-purity silicon, Nat. Mater. **11**, 143 (2012).

[69] J. T. Muhonen, J. P. Dehollain, A. Laucht, F. E. Hudson, R. Kalra, T. Sekiguchi, K. M. Itoh, D. N. Jamieson, J. C. McCallum, A. S. Dzurak, and A. Morello, Storing quantum information for 30 s in a nanoelectronic device, Nat. Nanotechnol. **9**, 986 (2014).

[70] M. Veldhorst, J. C. C. Hwang, C. H. Yang, A. W. Leenstra, B. de Ronde, J. P. Dehollain, J. T. Muhonen, F. E. Hudson, K. M. Itoh, A. Morello, and A. S. Dzurak, An addressable quantum dot qubit with fault-tolerant control-fidelity, Nat. Nanotechnol. **9**, 981 (2014).

[71] M. A. Nielsen and I. L. Chuang, *Quantum Computation and Quantum Information* (Cambridge University Press, Cambridge, UK, 2010).

[72] D. Klauser, W. A. Coish, and D. Loss, Nuclear spin state narrowing via gate-controlled Rabi oscillations in a double quantum dot, Phys. Rev. B **73**, 205302 (2006).

[73] L. Jiang, J. S. Hodges, J. R. Maze, P. Maurer, J. M. Taylor, D. G. Cory, P. R. Hemmer, R. L. Walsworth, A. Yacoby, A. S. Zibrov, and M. D. Lukin, Repetitive readout of a single electronic spin via quantum logic with nuclear spin ancillae, Science **326**, 267 (2009).

[74] P. London, J. Scheuer, J.-M. Cai, I. Schwarz, A. Retzker, M. B. Plenio, M. Katagiri, T. Teraji, S. Koizumi, J. Isoya, R. Fischer, L. P. McGuinness, B. Naydenov, and F. Jelezko, Detecting and Polarizing Nuclear Spins with Double Resonance on a Single Electron Spin, Phys. Rev. Lett. **111**, 067601 (2013).

[75] N. C. Menicucci, P. van Loock, M. Gu, C. Weedbrook, T. C. Ralph, and M. A. Nielsen, Universal Quantum Computation with Continuous-Variable Cluster States, Phys. Rev. Lett. **97**, 110501 (2006).

[76] R. Raussendorf and H. J. Briegel, A One-Way Quantum Computer, Phys. Rev. Lett. **86**, 5188 (2001).

[77] J. F. ¡johannes.feist@gmail.com¿ and contributors, Quantumalgebra.jl (2021).

[78] M. Sánchez-Barquilla, R. E. F. Silva, and J. Feist, Cumulant expansion for the treatment of light-matter interactions in arbitrary material structures, J. Chem. Phys. **152**, 034108 (2020).